Research Square

Preprints are preliminary reports that have not undergone peer review.
They should not be considered conclusive, used to inform clinical practice,
or referenced by the media as validated information.

Integrating laboratory-based secondary precipitation thresholds with ocean biogeochemistry models to advance ocean alkalinity enhancement decision-making

Allison Savoie

allison.savoie@pnnl.gov

Pacific Northwest National Laboratory https://orcid.org/0000-0003-0235-9503

Kyle Hinson

Pacific Northwest National Laboratory

Ashley Bird

Pacific Northwest National Laboratory https://orcid.org/0000-0002-1286-3116

Mallory Ringham

Emma Scott

Jessica Cross

Chinmayee Subban

Pacific Northwest National Laboratory

Alexa Labossiere

Remi Pages

University of Alaska Fairbanks https://orcid.org/0000-0002-3896-5372

Jilian Xiong

Zhaoqing Yang

Pacific Northwest National Laboratory https://orcid.org/0000-0001-9257-0796

Nicholas Ward

Pacific Northwest National Laboratory https://orcid.org/0000-0001-6174-5581

Article

Keywords:

Posted Date: August 26th, 2026

DOI: https://doi.org/10.21203/rs.3.rs-10639502/v1

License: This work is licensed under a Creative Commons Attribution 4.0 International License.
Read Full License

Additional Declarations: Yes there is potential Competing Interest. Author MR was employed by Ebb Carbon, Inc. The remaining authors declare that the research was conducted in the absence of any commercial or financial relationships that could be construed as a potential conflict of interest.

Title: Integrating laboratory-based secondary precipitation thresholds with ocean biogeochemistry models to advance ocean alkalinity enhancement decision-making

Authors: Allison M. Savoie[1*], Kyle E. Hinson[1], Ashley Bird[1], Mallory Ringham[2], Emma Scott[1], Jessica N. Cross[1,3], Chinmayee Subban[1,4], Alexa K. Labossiere[5], Rémi Pagès[6], Jilian Xiong[7], Zhaoqing Yang[1], Nicholas D. Ward[1,3]

1- Pacific Northwest National Laboratory, Coastal Sciences Division, Sequim, WA
2- Ebb Carbon, Inc., South San Francisco, CA
3- University of Washington, School of Oceanography, Seattle, WA
4- Department of Materials Science and Engineering, University of Washington, Seattle, WA
5- Virginia Institute of Marine Science, William & Mary, Gloucester Point, VA
6- International Arctic Research Center, University of Alaska Fairbanks, Fairbanks, AK
7- Woods Hole Oceanographic Institution, Woods Hole, MA

*Corresponding Author – Allison M. Savoie can be contacted at allison.savoie@pnnl.gov

Abstract

Ocean alkalinity enhancement (OAE) is a promising marine carbon dioxide removal strategy, yet its effectiveness depends on avoiding secondary abiotic precipitation that reduces alkalinity and carbon uptake. We conducted controlled microcosm experiments across temperature (7.5–29.5 °C) and salinity (6.5–32.5) gradients to quantify NaOH-driven precipitation thresholds relevant to coastal OAE deployments. Higher temperatures accelerated precipitation and lowered the Ω_{ar} threshold for precipitation, while lower salinities led to shifts in mineralogy mediated by pH, DIC, and Mg/Ca stoichiometry. Ω_{ar} thresholds for $CaCO_3$ formation were substantially higher than previously reported, and runaway precipitation occurred only at temperatures ≥ 16 °C under high alkalinity additions. Integrating experimentally-derived, temperature- and salinity-dependent saturation thresholds into a regional biogeochemical model produced substantial, spatially variable reductions in added alkalinity and atmospheric CO_2 uptake. These results provide operational bounds for safe and efficient OAE implementation and highlight the necessity of explicit precipitation parameterizations in predictive modeling frameworks.

1.0 Introduction

Climate change strategies that incorporate active carbon removal technologies are necessary for avoiding the worst impacts of climate change[1-3]. Among marine-based carbon dioxide removal (mCDR) pathways, ocean alkalinity enhancement (OAE) shows potential for scalable CDR[4,5]. OAE alters seawater carbonate chemistry by elevating alkalinity in seawater, thereby decreasing the partial pressure of CO_2 in seawater and prompting atmospheric CO_2 to

diffuse into the water to restore equilibrium across the air-sea boundary[4-6]. This method enhances uptake of atmospheric CO_2 and/or decreases degassing of CO_2 to the atmosphere, leading to durable carbon storage the form of bicarbonate.

Multiple OAE approaches exist, including the addition of solid alkaline materials to seawater or electrochemically converting seawater or brine into alkaline solutions[6,7]. Herein, we focus on the latter, using laboratory experiments to test the stability of an aqueous alkalinity solution added to seawater. Electrochemical alkalinity generation has been described previously[7-11]. One electrochemical OAE pathway uses bipolar membrane electrodialysis to remove acid from seawater or brine and returns alkalinity or an alkalinity-enhanced seawater stream to the surface ocean. The chemistry in this pathway is analogous to the addition of NaOH to seawater, which has been used in multiple laboratory and mesocosm studies of OAE efficiency and impacts[12-24], field trials[8,25-27], and has been developed within a research pilot by Ebb Carbon, Inc.[28]. As NaOH is added to seawater, the increase in seawater pH rapidly shifts dissolved inorganic carbon (DIC) speciation towards carbonate (Eq. 1)[7]:

$$OH^- + HCO_3^- \rightarrow H_2O + CO_3^{2-} \quad (1a)$$

$$OH^- + CO_{2,aq} \rightarrow HCO_3^- \quad (1b)$$

This lowers the concentration of dissolved CO_2 gas ($CO_{2,aq}$) in solution relative to atmospherically equilibrated seawater. Over weeks to years [10,29-31], CO_2 re-equilibrates across the air-sea boundary and is stored primarily as bicarbonate (Eq. 2)[5,7,12,32,33]:

$$CO_{2,g} \rightarrow CO_{2,aq} \quad (2a)$$

$$CO_{2,aq} + CO_3^{2-} + H_2O \rightarrow 2HCO_3^- \quad (2b)$$

Under typical ocean conditions, OAE causes the ocean to absorb ~ 0.7 – 0.9 mol of DIC per mol of NaOH added[10,12,29-31], rather than the theoretical 1:1 maximum. Efficiency decreases when added alkalinity cannot interact with the atmosphere due to sinking, subduction, or secondary precipitation that mineralizes or re-mineralizes dissolved alkalinity. Some inefficiency may also occur when added alkalinity suppresses natural alkalinity production[7,30,34].

Secondary inorganic precipitation of brucite ($Mg(OH)_2$) and calcium carbonate ($CaCO_3$) is likely to occur to some extent, however some alkalinity delivery strategies can favor large-scale precipitation[5,12,17,35-38]. This precipitation can result in a significant loss of added alkalinity from solution and increase turbidity/total suspended solids, potentially impacting photosynthesis and predator-prey dynamics. Surface seawater typically exists in a metastable supersaturated state with respect to $CaCO_3$ in the form of calcite and aragonite, and spontaneous $CaCO_3$ precipitation is rare. $CaCO_3$ solubility (Ω) is defined in Eq. 3, where K_{sp} is the solubility product of $CaCO_3$ which is dependent on ambient temperature, salinity, and pressure[39]:

$$\Omega = \frac{[Ca^{2+}][CO_3^{2-}]}{K_{sp}} \quad (3)$$

$CaCO_3$ solubility decreases with increasing temperature[40] and increases with increasing salinity due to decreased ion activity coefficients for Ca^{2+} and CO_3^{2-} in solutions with increasing ionic strength (i.e. higher salinity)[39]. Precipitation also depends on the availability of suspended nuclei, residence time at elevated saturation states, and inhibition by magnesium or dissolved inorganic matter [18,37,41,42]. Alkalinity addition can result in sufficiently high supersaturation where kinetic inhibition is overcome and trigger rapid precipitation; in some cases, there is a positive feedback process in which more alkalinity is lost from solution than was initially added[12,16,17]. $Mg(OH)_2$ can readily redissolve under standard seawater conditions but $CaCO_3$ does not. OAE projects

must quantify the loss of added alkalinity to both minerals to accurately calculate net carbon removed by the project over time (Isometric, 2026). Given the novelty of OAE deployment, it is therefore useful to identify local conditions under which secondary precipitation is likely, allowing developers to design engineering controls to limit or avoid precipitation.

Currently, regional ocean biogeochemistry models assess OAE by tracking air–sea gas exchange through the model domain following alkalinity addition and comparing it to a baseline without intervention to determine gross and net CDR (after also removing project emissions)[43-46]. Current models do not incorporate secondary precipitation and may overestimate carbon sequestration by an OAE intervention when secondary precipitation does not redissolve in the surface ocean[43,44]. Incorporating precipitation dynamics into regional models requires careful consideration of scale, in that point-source releases of alkalinity require high resolution models to account for rapidly changing precipitate conditions. Models will need to parameterize mineral precipitation (both mineral composition and rate), dissolution rate, particle sinking speeds, and when precipitation calculations are relevant to capture the impact of secondary precipitation on carbon removal. Laboratory studies that identify saturation state thresholds for precipitation can help identify conditions for concern and enable conservative calculations of alkalinity losses. The experiments presented here were designed to directly inform such model parameterizations of secondary precipitation.

We conducted 48-hour saturation state threshold experiments by adding electrochemically generated alkalinity to natural seawater sourced from Sequim Bay, WA, USA, which was modified for varied temperature (7.5 - 29.5 ˚C) and salinity (6.5 - 32.5) cases. Our goals were to: (1) to fill a knowledge gap in OAE precipitation kinetics and useable OAE thresholds across coastal environmental conditions; (2) integrate NaOH precipitation thresholds

into OAE model simulations using our experimental and literature data to better inform regional scale modeling efforts for OAE deployments; and (3) test precipitation impacts on CDR through a hypothetical, large-scale OAE deployment within a well-validated regional model (Figure 1).

We show secondary precipitation rates increased with increasing temperature, similar to prior work. Precipitation generally increased with decreasing salinity, which also impacted the type of mineral precipitated. Observed thresholds for precipitation were high relative to some previous literature[16,17,37,40,47]. Experimental data and literature-derived precipitation model parameterizations were then applied to a well-validated regional model in the Chesapeake Bay, chosen because it spans the full temperature and salinity ranges tested, whereas Sequim Bay has a smaller range of variability. Together, this work provides a framework for 1) assessment of conservative secondary precipitation thresholds for NaOH-based OAE, 2) integration of precipitation into ocean biogeochemistry modelling, and 3) guidance for refining laboratory and field observations of precipitation dynamics, along with considerations for relevant model scales.

2.0 Materials & Methods

2.1 Experimental Setup

Two experiments were used to evaluate the threshold saturation states and timing of secondary precipitation triggered by the addition of NaOH-based alkalinity to seawater under conditions of varying temperature or salinity. The experiment with varied temperature was conducted between June and August 2025 (Section 2.2) and the experiment with varied salinity was conducted between September and October 2025 (Section 2.3). During each experiment, eight 8 L rectangular microcosm tanks were filled with 7.5 L seawater collected during flood

tides from the Pacific Northwest National Laboratory facility intake from Sequim Bay, WA, US (Figure 1). The eight tanks were divided evenly into an 'unfiltered' set of 4, in which raw seawater was collected from the facility intake, and a 'filtered' set of 4, in which the same seawater source was filtered with 0.45 μm GF/F filters to reduce the influence of biology. The tanks were triple conditioned with raw or filtered seawater prior to being filled and then were left to equilibrate for a given temperature and salinity in a water bath overnight. One tank within each set was designated as a control, and the remaining three tanks in each set were treated with alkalinity, as described below. The tanks were monitored for 48 hours and then were reset for testing at the next temperature and salinity of interest.

The purpose of testing unfiltered versus filtered conditions was to separate the potential impacts of: 1) small, suspended particulates on precipitation dynamics, given that particulates can provide nucleation surfaces that reduce the activation energy of initial precipitation; 2) dissolved organic matter that can potentially inhibit precipitation by occupying nucleation sites; and 3) seawater carbonate chemistry that may be altered via photosynthesis and respiration. Due to logistical constraints these factors could not be comprehensively studied in these experiments, so the bulk effects of filtration were captured to inform future research priorities.

Electrochemically-generated NaOH was used as the alkalinity source for these experiments. Briefly, an Ebb Carbon bipolar membrane electrodialysis system was installed at the Pacific Northwest National Laboratory in Sequim, WA in 2023, and has been used in a series of prior experiments[8,10,19]. Seawater sourced from the PNNL facility was concentrated into an aqueous brine and passed through the electrodialysis process to produce acid (HCl) and base (NaOH) streams[7]. System tests show that the concentration of acid and base products can be

variable, so all experiments described in this study used a single batch of NaOH with concentration 0.5 mol L^{-1}.

NaOH was added to each of the 3 test tanks in the unfiltered and filtered tanks to raise the total alkalinity (TA) of seawater by: +0 µmol kg^{-1} (control tank), +1500 µmol kg^{-1} (low), +2500 µmol kg^{-1} (medium), and +3500 µmol kg^{-1} (high). The tanks were continuously and gently bubbled with ambient air, which served to thoroughly mix NaOH into seawater while rapidly redissolving any initial brucite precipitate. Bubbling rates were not available for the simple aquarium systems used, but all settings were held constant across tanks and between experiments.

Sample and sensor data was used to assess resulting secondary precipitation. Discrete bottle samples were collected for TA and dissolved inorganic carbon (DIC) analysis from each control tank in the unfiltered and filtered tanks prior to the alkalinity addition (t_0), and the average t_0 control tank measurement was assumed to represent the initial carbonate chemistry of all remaining tanks. After alkalinity addition, bottle samples for TA and DIC were collected as soon as any initial brucite precipitation was visibly dissolved (t_1), aat 3 hours (t_3), at 24 hours (t_{24}), and at 48 hours (t_{48}) after the alkalinity addition. All samples were filtered with 0.45 µm GF/F filters and pumped into 100 mL borosilicate glass bottles following procedures from Dickson, et al. [48]. The samples were immediately poisoned with 50 µL of a fully saturated $HgCl_2$ solution. TA and DIC samples were analyzed on the day of collection to limit secondary precipitation in the bottles, as described in Section 2.4.

YSI ProDSS sondes were used to continuously measure seawater temperature, salinity, turbidity, and pH (A complete table of measurements is included in the supplemental materials (SM. 1-2)). The sondes were calibrated weekly on the day of seawater collection for each

experiment using OSIL Atlantic Seawater Standard (conductivity), Orion pH buffers (4.01, 7.00, and 10.01), and a YSI turbidity standard (124.00). The accuracy and precision of these sondes is reported by YSI as ±0.5% of reading or 0.001 mS/cm, whichever is greater for conductivity, ±0.2 units for pH, and ±0.3 or ±2% of reading, whichever is greater for turbidity.

Solid samples were collected after the alkalinity addition and redissolution of any initial brucite precipitation, at the first visual evidence of additional precipitation (i.e. water cloudiness, whitening, snow or crystal-like solids). Samples were then collected ~24 and ~48 hours after base addition. Samples were collected by filtering at least 500 mL of water onto a 0.45 μm Millipore Durapore filter. The filter was triple rinsed with DI water, precipitates were removed from the filter using a sterile disposable spatula, placed in an oven-proof vial, and dried at 80˚C overnight or for at least 12 hours. A subset of the samples was ground with a mortar and pestle for analysis using x-ray diffraction (XRD, D8 Discover Microfocus, Bruker) and scanning electron microscopy (SEM, Apreo 2S SEM, ThermoFisher Scientific) (Section 2.4).

After the end of each experiment, tanks were drained and any precipitates that adhered to tank walls were removed by scraping/scrubbing with a 10% HCl rinse or soak, followed by a triple rinse with DI water. If precipitate buildup was substantial, tanks were first soaked with liquinox and DI water prior to the acid rinse. Tanks were then rinsed with ambient unfiltered or filtered seawater before refilling for each subsequent experiment.

2.2 Experiment One: Temperature variation during alkalinity addition

During the first experiment series, temperature was varied while salinity and all other factors, with the exception of the timing of seawater sourcing, were held constant. This

experiment was conducted over a period of 5 weeks from June to August 2025, during which time average temperature and salinity measured at a dock ~35m from the seawater intake within Sequim Bay were 12.7 ± 1.9˚C and 31.00 ± 0.10, respectively. Average initial salinity of the seawater across the experiment was 32.31 ± 0.77, therefore, salinity increased slightly from ambient conditions while equilibrating to the controlled laboratory and water bath temperatures.

One round of testing was completed each week in which temperatures were controlled (±0.5˚C) within a freshwater bath, consisting of an insulated tote with copper tubing from an external pumped VWR water heater/ chiller. Temperatures were increased between each round of tests at steps of: ~7.5˚C, 11˚C, 16˚C, 21˚C, 29.5˚C. These temperatures were chosen to be representative of the coastal region and conditions of interest for future OAE deployments. Salinity remained constant across the experiment for all temperature groups, except for the T = 29.5°C group, which had a slight increase in salinity over the experiment that likely resulted from increased evaporation (Table 1).

208 *Table 1*. **Average temperature and salinity conditions across both laboratory experiments**
209 **and model simulations in the Chesapeake Bay**. Mean monthly temperature and salinity
210 conditions with standard deviations are provided for the precise cell at which alkalinity was
211 added for model scenarios.

Experiment	Analysis Site	Group	Average Starting Salinity	Average Salinity Across Experiment	Average Temperature (°C)
1	Sequim Bay	7.5	32.69 ± 0.28	32.62 ± 0.28	7.64 ± 0.15
		11	32.55 ± 0.15	32.58 ± 0.16	10.92 ± 0.20
		16	31.38 ± 0.20	31.46 ± 0.18	16.18 ± 0.27
		21	31.63 ± 0.14	31.90 ± 0.12	21.05 ± 0.31
		29.5	33.33 ± 0.43	34.10 ± 0.43	29.49 ± 0.48
		Entire Experiment	32.31 ± 0.77	32.56 ± 1.21	Variable
2	Sequim Bay	6.5	6.52 ± 0.12	6.54 ± 0.11	9.91 ± 0.10
		12.5	12.46 ± 0.23	12.49 ± 0.25	10.32 ± 0.23
		18.5	18.54 ± 0.35	18.55 ± 0.37	9.73 ± 0.20
		24.5	24.32 ± 0.20	24.36 ± 0.20	9.61 ± 0.14
		32.5	32.35 ± 0.45	32.34 ± 0.47	10.05 ± 0.28
		Entire Experiment	Variable	Variable	9.90 ± 0.37
Model Simulations in Chesapeake Bay	Baltimore Harbor	January 2024	N/A	8.7 ± 1.1	4.9 ± 1.2
		June 2024	N/A	6.9 ± 0.8	25.6 ± 2.4
	Southern Bay	January 2024	N/A	20.1 ± 0.8	5.9 ± 0.8
		June 2024	N/A	17.4 ± 0.2	26.5 ± 1.3

212

213 *2.3 Experiment Two: Salinity variation during alkalinity addition*

214 During the second experiment, all tanks were held at 9.9 ± 0.4 ˚C, similar to average
215 ambient seawater conditions of Sequim Bay (Table 1). This experiment was conducted from

September to October 2025, during which time average temperature and salinity prior to alteration for Sequim Bay were 11.9 ± 0.6˚C and 31.68 ± 0.19. Experiment 2 took place over a period of 5 weeks, during which salinity was adjusted to steps of ~6.5, 12.5, 18.5, 24.5, and 32.5 by dilution with DI water. Each salinity group was prepared as a large, homogenized batch and then measured and distributed to each tank either with or without filtration.

2.4 Sample Analysis & Data Processing

TA was analyzed on an Apollo SciTech Total Alkalinity Titrator (AS-ALK3) using the Gran Titration Method. DIC was analyzed on an Apollo SciTech Dissolved Inorganic Carbon Analyzer (Model: AS-C6L). These instruments were calibrated using certified reference materials (CRMs) supplied by the Dickson laboratory at Scripps Institution of Oceanography (Batch #206). The precision of these instruments based on repeated measurements of the CRMs was ±1 μmol kg^{-1} for TA and ±2 μmol kg^{-1} for DIC. The average standard deviation across all replicate analyses of experiment samples was ±3 μmol kg^{-1} for TA and ± 1 μmol kg^{-1} for DIC. Carbonate system data was calculated from TA and DIC data using the MATLAB version of CO2SYS, using K_1 and K_2 from Millero [49], KSO_4 dissociation constant from Dickson [50], KF dissociation constant from Perez and Fraga [51], and borate-to-salinity ratio from Lee, et al. [52].

The bubblers in the tanks interfered with YSI data at some time points and so to account for this a detailed outlier flag and removal was done by calculating the z-score of each data point and removing any data point with z>3. Data from the LISST-200X PSA was post-processed in MATLAB using the *getscat_L200X* function provided by Sequoia. The PSA collected 1 sample per second for ~60 seconds for each tank at each time point. Each data cluster (~60 points) was

filtered to remove any points with optical transmission values > 99.5% or < 30% (per manufacturer instructions) and then filtered for outliers. The average diameter and total concentration were calculated from the remaining data to get one value per tank at each sampling time point.

XRD was used to characterize filtered sample structure and phase using a Cu Kα radiation source (λ = 1.54184 Å). The 2D patterns were integrated to generate 1D spectra for analysis. Jade Pro (MDI) software was used for analysis. Morphology was imaged using scanning electron microscopy (SEM, Apreo 2S SEM, ThermoFisher Scientific). Samples were mounted on carbon tape and coated with 4 nm carbon using a sputter coater (EM ACE 600, Leica) prior to imaging. Images were collected at 2 kV and 13 pA. Energy dispersive X-ray spectroscopy (EDS, Octane Elite, EDAX) at 20 kV and 1.6 nA under low vacuum (80 pascal to mitigate charging) was used for elemental analysis. Due to relatively small sample size and potential costs, not all samples were analyzed across all three methods. A complete table with each solid sample and the analysis conducted is included in the supplemental materials (SM. 3).

2.5 Incorporation of Precipitation in an Ocean Biogeochemistry Model

An accessible regional ocean modeling system configuration of Chesapeake Bay biogeochemistry (ROMS-ECB)[53] was used to test the impacts of secondary precipitation within a realistic domain. While we recognize that the previous section's experiments were conducted with seawater from Sequim Bay and this location is not necessarily directly applicable to other conditions and locations, here we chose to develop and test the secondary precipitation module in Chesapeake Bay because it conditions there cover a wider range of temperatures and salinities

of interest, where Sequim Bay has a smaller range of natural variability. Both Sequim Bay and the Chesapeake Bay have had OAE field trials completed or in planning[8] (https://www.umces.edu/impacting-ocean-alkalinity/), and regional models in these locations have been used to represent both real and hypothetical OAE deployments[10,54]. ROMS-ECB has an average horizontal resolution of 600 m with 20 terrain-following vertical depth levels and represents the nitrogen and carbon cycles, sinks and sources of dissolved oxygen, bottom biogeochemical fluxes, and air-sea exchanges. The model was run using realistic atmospheric forcings, riverine inputs, and boundary conditions as described by St-Laurent and Friedrichs [53] for month-long periods in January and June of 2024, representing winter and summer conditions, respectively, to test the range of temperatures used in our experiments. In addition to a baseline simulation, two sets of alkalinity addition scenarios were simulated with surface fluxes of alkalinity at two locations within the Chesapeake Bay, both applied to a single grid cell (0.36 km^2) of the model domain to test NaOH injections in areas with differing salinities (Table 1).

Model simulations applied a large increase in the surface flux of alkalinity over the course of the first day of OAE model simulations at a rate of 4.05 mmol m^{-2} s^{-1} (equivalent to 126.0 Mmol alkalinity released over the 1-day addition period). This extremely high addition was chosen to ensure that the thresholds necessary to trigger secondary precipitation would be distinguishable in the modeled open-system environment. Lower alkalinity flux concentrations that experienced rapid dilution and mixing among surrounding and subsurface model grid cells would prohibit further analysis of secondary precipitation phenomena. Compared to other work, this is a significantly scaled intervention: a study by Khangaonkar, et al. [10] simulated electrochemical OAE in Sequim Bay from a continuously operating 1000x pilot scale, with a maximum alkalinity discharge of 164 Mmol alkalinity added over the course of 1 year. Our

simulation here added a similar amount of alkalinity over the course of a single day. This exercise should therefore be understood to represent how secondary precipitation may be modeled, and not to indicate the potential for alkalinity loss during the current or future expected scale of OAE operations. Our simulation is entirely hypothetical, separate from existing outfalls or CDR proposals in the region, and does not consider practical or regulatory considerations associated with elevated pH at the point of release.

OAE model scenarios included the addition of a surface source of alkalinity, with one set of simulations (OAE) accounting for the distribution and resulting carbon uptake due to alkalinity addition, and the second set (OAE + 2° Precipitation) incorporating secondary precipitation that acted as a temporary sink of total alkalinity and dissolved inorganic carbon (CO_3^{2-}), following the methodology of Hinson et al. (*in prep*). In brief, this approach first calculates the aragonite saturation state (Ω_{ar}) of a given model cell where the added surface flux of alkalinity is present and determines whether Ω_{arag} exceeds the threshold (Ω_{thresh}) for secondary precipitation to immediately occur in the model grid cell. The Ω_{thresh} value was determined through an analysis that was based on the findings from this work and that of Ringham, et al. [12] on precipitation thresholds. Because Ω_{thresh} varies with temperature and salinity, we derived a logistic regression model using experimental temperature, salinity, and peak Ω_{ar} from both experimental data sets at a probability of 0.5. The logistic decision boundary was defined as $p = 0.5$, the point where the model was equally likely to indicate precipitation occurred ($p \geq 0.5$) or precipitation did not occur ($p < 0.5$). The logistical model informs the activation of secondary precipitation within simulations at each time step. It is important to note that the Ω_{thresh} was not equivalent to the physicochemical saturation state equation and also does not imply that Ω depends solely on temperature and salinity. Rather, Ω_{thresh} was an empirical precipitation

threshold dependent on environmental conditions, because the peak of measured Ω_{ar} from this work's experimental data already embedded carbonate chemistry interactions. Therefore, the logistic regression model represents values of Ω_{thresh} at which secondary precipitation is triggered as a function of temperature and salinity.

The logistic regression first categorized conditions where secondary precipitation was identified as a substantial loss in $\Delta TA \geq 400$ μmol kg^{-1} for experiment 1 and ≥ 200 μmol kg^{-1} for experiment 2. This value was selected as representative of the experimental data where precipitation was observed by metrics including visual whiting, crystalline formation, and increased turbidity. We note that this is not a comprehensive metric and likely will not transfer to other experiments or field sites, based on varied conditions including alkaline addition rates and methods, suspended sediments, air bubbling and mixing, and other factors, but serves as a valuable benchmark for this initial simulation. We then incorporated temperature, salinity, and peak Ω_{ar} data from experimental conditions to use alongside the categorical precipitation variable. This was done using the following equation:

$$logit(p) = \beta_0 + \beta_T(T - T_{ref}) + \beta_S(S - S_{ref}) + \beta_{TS}(T - T_{ref})(S - S_{ref}) + \beta_\Omega\, \Omega_{peak,th} \quad (4a)$$

Solving for the Ω value that resulted in **p = 0.5**, logit(0.5) = 0, the resulting expression was rearranged to:

$$\Omega_{thresh}(T,S) = -\frac{\beta_0+\beta_T(T-T_{ref})+\beta_S(S-S_{ref})+\beta_{TS}(T-T_{ref})(S-S_{ref})}{\beta_\Omega} \quad (4b)$$

where Ω_{thresh} (T,S) represented the aragonite threshold function at a given temperature and salinity, β_0 was the baseline Ω threshold (-37.6711), β_T was a measure of temperature shifting Ω_{thresh} (0.4165), β_S was a measure of salinity shifting Ω_{thresh} (-0.8402), β_{ST} represented the interaction term between temperature and salinity (-0.0096), β_Ω was a measure of the effect of Ω

on precipitation probability (1.1458), and the reference values of temperature and salinity were set (T_{ref} = mean T across Experiment 2 = 9.97 °C; S_{ref} = mean S across Experiment 1 = 32.35). All β values were empirically derived from the experimental data presented in this work and that reported in Ringham, et al. [12] to provide data coverage in the 16-22 °C and 27-32 °C range respectively.

An error uncertainty analysis was also performed on the original logistical regression using the delta method and then again on the data set after bootstrapping 500 times (i.e. creating a synthetic dataset by randomly sampling the original dataset with replacement). The results of the error analysis are shown in SM. 4. After this logistical regression model was incorporated within the ROMS-ECB simulations to represent Ω_{thresh}, the model modified the native biogeochemical fields of dissolved inorganic carbon and alkalinity following the methodology of Hinson et al. (in prep). The loss of CO_3^{2-} from a model grid cell where secondary precipitation was triggered followed the decay rate reported by Hashim, et al. [47].

It is important to note that this method identified precipitation-relevant conditions and began simulating the loss of carbonate from solution immediately: this method did not account for potential induction times or lag times in carbonate mineral formation as identified by Suitner, et al. [18], Ringham, et al. [12], and others. It is also important to note that this module handled carbonate chemistry only, neglecting $Mg(OH)_2$ or other mineral formation that may impact carbonate chemistry and other factors relevant to carbonate mineral precipitation. Where the model triggered precipitation, particulate was assumed to form at size 8-12 μm (Section 3.3 (SEM data)) and was set to sink at a rate of 2 meters per day. This was a conservative estimate based on findings from Suitner, et al. [18], which observed rates ~5 m d^{-1} for larger particles at 14 μm, and Bach, et al. [55] with ranges of 0.3 – 4.3 m d^{-1} for various calcifying phytoplankton.

Additionally, because precipitation (and the loss of additional CO_3^{2-}) may continue even if Ω_{ar} drops below Ω_{thresh}, as observed with runaway precipitation, then further precipitation was permitted if secondary precipitate particles were present from the previous time step within the alkaline plume. This continued until Ω_{ar} <5, approximately representing conditions where runaway precipitation ceased based on previous research [12,16-18]. If Ω_{ar} fell below 1, the secondary precipitate was instantly remineralized and reallocated to the TA and DIC pools in a 2:1 ratio within whatever grid cell it occupied.

3.0 Results

3.1 Experiment One – Temperature variation during alkalinity addition

Precipitation increased with temperature, consistent with $CaCO_3$ solubility trends (Eq. 3b). Filtered and unfiltered results were similar except at T = 7.5 °C (Figure 2). In this case, the high alkalinity treatment in the filtered seawater tank produced TA and DIC losses from solution over time, indicative of abiotic precipitation (Figure 2A & 2F; Table 2), although no visual evidence (i.e. solids or increased turbidity) was observed. The unfiltered seawater tank had slower TA loss and an increase in DIC throughout the experiment (Figure 2A & 2F; Table 2), again without visual or turbidity evidence of precipitation. At T = 16 °C, both filtered and unfiltered tanks had precipitation as indicated by both decreased TA and DIC data along with visual observations (Figure 2C & 2H; Table 2). 'Runaway' precipitation occurred at the highest alkalinity treatments starting at 16°C and warmer, in which more DIC and TA were lost from solution than were present before the alkalinity addition, and accelerated with increasing temperature (Figure 2 C – E & 2 H – J; Table 2).

In the highest alkalinity addition (+3500 µmol kg^{-1}), peak Ω_{ar} was ~33–36 across temperature groups before precipitation (Figure 2K–O; Table 2). Medium treatments (+2500 µmol kg^{-1}) reached $\Omega_{ar} \approx 30$ for all temperature groups; low treatments (+1500 µmol kg^{-1}) peaked at $\Omega_{ar} \approx 20$ (Figure 2K–O). The medium alkalinity treatment tanks remained stable across the experiment even at significantly elevated Ω_{ar} ($\leq$30) until T = 29.5 °C, where slow precipitation occurred in both filtered and unfiltered tanks (Figure 2E & 2J). Low alkalinity treatments did not result in precipitation under any temperature group by either visual evidence or seawater carbonate chemistry analysis (Figure 2). Small TA decreases with corresponding DIC increases likely reflected CO_2 equilibration rather than precipitation (Figure 2A–D; 2F–I).

Table 2. **Precipitation data for high alkalinity (+3500 µmol kg^{-1}) treatment tanks across both experiments**.

Exp #	Temp (°C)	Sal	Timeline for observed precip	Peak Ω_{ar}	ΔΩar (max-min)	Filtered Tank Precip Rate (µmol hr^{-1})	Unfiltered Tank Precip Rate (µmol hr^{-1})
1	7.5	32	~Day	Filtered: 36 Unfiltered: 36	Filtered: 20 Unfiltered: 17	t_1 to t_3: +13 t_3 to t_{24}: -32 t_{24} to t_{48}: -22	t_1 to t_3 +10 t_3 to t_{24}: -12 t_{24} to t_{48}: -9
	11	32	Hours-Day	Filtered: 35 Unfiltered: 36	Filtered: 10 Unfiltered: 15	t_1 to t_3: -10 t_3 to t_{24}: -11 t_{24} to t_{48}: -7	t_1 to t_3: +4 t_3 to t_{24}: -7 t_{24} to t_{48}: -5
	16	32	Hours	Filtered: 34 Unfiltered: 34	Filtered: 29 Unfiltered: 30	t_1 to t_3: -47 t_3 to t_{24}: -71 t_{24} to t_{48}: -8	t_1 to t_3: -49 t_3 to t_{24}: -77 t_{24} to t_{48}: +2
	21	32	Hours	Filtered: 34 Unfiltered: 34	Filtered: 29 Unfiltered: 31	t_1 to t_3: -73 t_3 to t_{24}: -73 t_{24} to t_{48}: -2	t_1 to t_3: -101 t_3 to t_{24}: -72 t_{24} to t_{48}: +1
	29.5	32	Minutes-Hour	Filtered: 33 Unfiltered: 34	Filtered: 30 Unfiltered: 31	t_1 to t_3: -568 t_3 to t_{24}: -9 t_{24} to t_{48}: +3	t_1 to t_3: -564 t_3 to t_{24}: -15 t_{24} to t_{48}: +6
2	9.5	7.5	~Day (for $CaCO_3$)	Filtered: 19 Unfiltered: 19	Filtered: 6 Unfiltered: 5	t_1 to t_3: -4 t_3 to t_{24}: +16 t_{24} to t_{48}: -7	t_1 to t_3: +68 t_3 to t_{24}: -4 t_{24} to t_{48}: -4
	9.5	12.5	Hours-Day (for $CaCO_3$)	Filtered: 18 Unfiltered: 19	Filtered: 3 Unfiltered: 6	t_1 to t_3: +10 t_3 to t_{24}: -5 t_{24} to t_{48}: -5	t_1 to t_3: +2 t_3 to t_{24}: -8 t_{24} to t_{48}: -8
	9.5	18.5	Hours	Filtered: 25 Unfiltered: 25	Filtered: 12 Unfiltered: 17	t_1 to t_3: -16 t_3 to t_{24}: -15 t_{24} to t_{48}: -16	t_1 to t_3: -19 t_3 to t_{24}: -19 t_{24} to t_{48}: -18
	9.5	24.5	Hours	Filtered: 31 Unfiltered: 31	Filtered: 7 Unfiltered: 10	t_1 to t_3: -21 t_3 to t_{24}: -7 t_{24} to t_{48}: -5	t_1 to t_3: -12 t_3 to t_{24}: -9 t_{24} to t_{48}: -2
	9.5	32.5	Hours	Filtered: 35 Unfiltered: 35	Filtered: 9 Unfiltered: 11	t_1 to t_3: -18 t_3 to t_{24}: -4 t_{24} to t_{48}: -7	t_1 to t_3: -18 t_3 to t_{24}: -1 t_{24} to t_{48}: -6

386 *3.2 Experiment Two – Salinity variation during alkalinity addition*

387 We hypothesized that lower salinity would increase precipitation by lowering ionic
388 strength, reducing Ksp, and raising saturation at a given temperature (Eq. 3b). This trend held
389 from S = 18.5 to 32.5, but not at S = 6.5 and 12.5 (Figure 3; Table 2). In high-alkalinity
390 treatments at S = 6.5 and 12.5, precipitation was not significantly greater than at S = 18.5 (Figure
391 3A–C, 3F–H; Table 2). Initial decreases in TA in the high alkalinity treatments in the S = 6.5 and
392 S = 12.5 groups were not accompanied by decreased DIC (Figure 3 A – B & 3 F – G), indicating
393 hydroxide (e.g., brucite) rather than carbonate precipitation. At S = 18.5, concurrent TA and DIC
394 decrease in the high alkalinity treatment indicated $CaCO_3$ formation (Figure 3C, 3H). TA and
395 DIC never fell below control values at any salinity or alkalinity level and did not occur in a
396 "runaway" fashion at any point (Figure 3).

397 At S = 6.5 and 12.5, the highest alkalinity treatment had a peak $\Omega_{ar} \approx 19$ (Figure 3K–L;
398 Table 2), which was achieved later (~t_{24}) than in experiment 1 or during higher salinity groups (t_1
399 or t_3), despite ongoing precipitation (Table 2). In high-alkalinity treatments, peak Ω_{ar} increased
400 with salinity from 19 at S = 6.5 to 35 at S = 32.5 (Figure 3K–O; Table 2), except the filtered tank
401 at S = 12.5 (peak Ωar = 18). Medium and low treatments' peak Ωar increased with salinity (~19–
402 31 and ~12–19, respectively; Figure 3K–O The amount of precipitation in the high alkalinity
403 treatments, as indicated by $\Delta\Omega_{ar}$ and precipitation rates, decreased from S = 18.5 to S = 32.5
404 (Figure 3 D – E & 3 I – J; Table 2). Medium and low treatments did not have significant
405 precipitation even at elevated Ωar (≤29; Figure 3).

406 *3.3 Precipitated Mineral Characterization*

407 NaOH addition to seawater initially formed $Mg(OH)_2$, which was rapidly redissolved
408 with mixing to keep alkalinity in solution for assessing later carbonate precipitation. Beyond this
409 point, aragonite was the primary mineral precipitated during experiment 1 across temperatures,
410 time after base addition, or filtration conditions (Figure 4A, SM. 5). The predominant crystal
411 shapes observed across all time points were stem and double-broccoli shaped, with occasional
412 spheres (Figure 5A). Mineral shapes did not vary significantly between unfiltered and filtered
413 tanks (SM. 6). Minerals ranged from ~8-15 μm long as determined by SEM (Figure 5).

414 During experiment two, the predominant mineral precipitated across the high alkalinity
415 additions treatments shifted with time and salinity (Figure 4B). At t_3 in the S = 6.5 group, brucite
416 was the dominate mineral precipitated as identified by XRD, SEM, and EDS mapping (Figure 4
417 – 6). EDS identified Mg and O, not Ca, unlike the precipitate samples collected at t_3 in
418 experiment one (Figure 6). Minerology shifted over time from only brucite at t_3 to solely
419 aragonite by t_{48} (Figure 4 – 6). At t_{24}, both brucite and aragonite were present, with aragonite
420 crystals forming on the brucite crystal surfaces (Figure 5 & 6). By t_{48}, aragonite crystals were
421 primarily fully developed spheres or needle-like structures (Figure 5). Brucite crystals were
422 much larger (100's of μm) than aragonite crystals (8 – 15 μm). Similar patterns in mineral
423 composition, size, and formation were observed between the unfiltered and filtered tanks (SM.
424 7). Insufficient precipitate was available at t_3 for S = 12.5 and 24.5, however t_{24} samples from S
425 = 12.5 were similar to the S = 6.5 group, while S = 24.5 resembled experiment one, with
426 primarily aragonite present in the XRD spectra (SM. 5).

427

3.4 Biogeochemical Model Results

Temperature conditions during the January simulation at both sites were closest to those from the T = 7.5 °C group (Baltimore Harbor = 4.9 °C; Southern Bay = 5.9°C; Table 1). During the June simulation, average temperatures for both sites were closest to the T = 29.5 °C group (Baltimore Harbor = 25.6 °C; Southern Bay = 26.5 °C; Table 1). Average salinity conditions at Baltimore Harbor were low in both January (S = 8.7) and June (S = 6.9), aligning them closer to the S = 6.5 group. In comparison, Southern Bay had higher average salinities in January (S = 20.1) and June (S = 17.4), that were most similar to the S = 18.5 group.

Including secondary precipitation in TA-addition simulations produced spatially and temporally variable TA and DIC differences (SM. 8-15). The greatest loss in TA between the simulations occurred within the first few days of the alkalinity release (Figure 7). In January, average TA across the plume decreased by 18.6% at Baltimore Harbor and 116.1% in Southern Bay with the addition of the 2˚ precipitation module(Figure 7 & 8; SM. 8 & 10). The largest average January TA differences were ~2 meq m^{-3} (≈2 µmol kg^{-1} at ρ = 1007 kg m^{-3}) in Baltimore Harbor and ~6 meq m^{-3} (≈6 µmol kg^{-1} at ρ = 1016 kg m^{-3}). Losses increased in June, where average TA decreased by 31.1% at Baltimore Harbor and 438.1% in Southern Bay (Figure 7–8; SM.9, 11). Peak June TA differences were ~6 meq m^{-3} (≈2 µmol kg^{-1} at ρ = 1002 kg m^{-3}) in Baltimore Harbor and ~55 meq m^{-3} (≈54 µmol kg^{-1} at ρ = 1010 kg m^{-3}) in Southern Bay. It is important to note that these values are averaged across the entire plume, near-source losses were often hundreds of meq m^{-3} (SM.8 – 11). TA losses due to secondary precipitation were greatest at the Southern Bay site during the warm, summertime conditions (Figure 8). In total, secondary precipitation reduced net air-sea CO_2 uptake by ~3.5 to 30% (or 174 kg to 3.34 metric tons) over one month between the OAE and OAE + 2° Precipitation simulations.

4 Discussion

4.1 Experimental and model results

Precipitation in this study required Ω_{ar} values much higher than best-practice guidance (Ω_{ar} > 12.3 at a salinity of 35 and temperature of 20 °C)[6,40]. High alkalinity additions (+3500 µmol kg^{-1}) precipitated across most of the temperature and salinity groups, with Ω_{ar} > 32 in the temperature experiment and at S ≥ 24.5. Lower salinity experiments had a threshold Ω_{ar} of ~19 before precipitation switched from dominantly brucite to dominantly aragonite. Runaway precipitation that reduced TA, DIC, and Ω_{ar} below baseline conditions occurred only in high alkalinity treatments ≥ 16 °C with Ω_{ar} > 32 (Figure 2).

Our results align with Ringham, et al. [12], who observed precipitation thresholds near Ω_{ar} ≈ 30 (NaOH alkalinity addition between +2216 and +2276 µmol; filtered; T = 16 – 21 ˚C and S = 26.8 – 30.4) in meso- and microcosm experiments. Closed-system studies reported lower thresholds of +1050 µmol kg^{-1} (Ωar ≈15 at T = 23 ˚C & S = 36.6) and +1400 µmol kg^{-1} (Ωar ≈ 17 at T = 10 – 11 ˚C & S = 32.6) with biology; +1200 µmol kg^{-1} (Ωar ≈ 15 at T=11 – 13 & S=32.6 and Ωar ≈19 at T=23.3 & S=36.6) without biology, respectively[16,17]. Another closed system study found precipitation at additions as low as Ωar ≤ 11 (+500 µmol kg^{-1} (T = 27 °C, S = 36)[47]. Open-system laboratory experiments, often at lower salinity but similar temperatures, diverged from closed-system thresholds, likely due to mixing and gas-exchange differences (e.g., air bubbling)[12,16,17]. This is supported by recent research where increased advection led to decreased $CaCO_3$ precipitation and a shorter critical alkalinity period for $CaCO_3$ formation during NaOH additions[37].

Filtered and unfiltered tests performed similarly except at T = 7.5 °C under high alkalinity, where the filtered tank had a greater TA & DIC loss than the unfiltered tank (Figure 2 & 3). This may be in part due to (1) higher respiration rates in the unfiltered tank, as the organic material was not filtered out; and (2) colder waters that were able to hold more of the respired CO_2 to help buffer the additional alkalinity compared to the filtered tank. This is similar to results from Fucich, et al. [20], which found that unsterilized alkalinity enhancement experiments had a consistently higher rate of equilibration than sterile experiments, potentially buffering carbonate shifts and limiting precipitation.

During the salinity experiment, precipitation did not occur at a rate fast enough nor at a quantity sufficient to bypass the initial baseline conditions (Figure 3; Table 2). Precipitation rates generally increased as salinity decreased from 32.5 down to 18.5 as expected based on Eq. 3 (Table 2). While we observed higher initial rates (t_3 to t_{24}) of precipitation in the S = 6.5 and 12.5 groups, the rates across the entire duration of the S = 18.5 group were higher and led to a larger overall decrease in TA and DIC (Table 2; Figure 3). Decreased precipitation in the S = 6.5 group is likely due to decreased ion concentration in the low salinity conditions. Even though lower ionic strength can enhance kinetic rates at a fixed Ω in theory[35], the ion concentrations may become limiting when salinity drops too low. At a salinity of 6.5, the $[Ca^{2+}]$ and $[Mg^{2+}]$ can be variable in estuarine and river influenced areas[56]. Dilution with freshwater also lowers the total available DIC, thereby reducing available $[CO_3^{2-}]$. Even after adding alkalinity to force supersaturation, the absolute moles of Ca^{2+} available limit how much $CaCO_3$ can form. Thus, at S = 6.5, the system may be Ca-limited, so the total $CaCO_3$ that can form is also limited. Whereas, at S = 18.5, $[Ca^{2+}]$ and $[Mg^{2+}]$ are sufficiently high for precipitation to proceed before those ions are consumed. Future work could investigate this further by directly measuring dissolved $[Ca^{2+}]$

and [Mg^{2+}] or by utilizing freshwater from different geologic basin types that have different starting TA, [Ca^{2+}], and [Mg^{2+}].

Mineral composition and morphology varied with salinity (Figure 4 – 6), while temperature controlled precipitation rates and quantity of precipitates (Table 2; Figure 2 & 3). Higher temperatures produced faster precipitation, greater concentration of precipitates, and lower Ω_{ar} thresholds for initial precipitate formation (Table 2; Figure 2). Aragonite was the dominant mineral precipitated across experiment 1 and the S = 18.5 to 32.5 groups of experiment 2 (Figure 4 – 6), excluding initial brucite formation during base addition that rapidly dissolved with mixing. However, at S = 6.5 and 12.5 brucite persisted from t_1 through t_{24} before transitioning to aragonite by t_{48} (Figure 4 – 6). Brucite's persistence at low temperature and salinity is consistent with reduced solubility with decreasing temperature[57]. Over time, as brucite formed this reduced the pH, while there was still an increasing pool of available DIC from the seawater component and via CO_2 uptake. Both factors, decreased pH and available CO_3^{2-} ions, led to decreased stability of brucite over time. Meanwhile, aragonite could still precipitate as the thermodynamic boundary for the reaction to proceed was met. The greater stability of aragonite relative to metastable brucite rendered it less likely to redissolve. Finally, brucite provided an initial nucleation surface for aragonite precipitation, as observed at t_{24} (Figure 4 – 6; SEM zoomed to 5 μm in SM. 20). Previous studies have proposed that initial brucite formation may act as a nucleating surface for aragonite precipitation, greatly reducing energetic barriers to initial particle formation and decreasing the critical saturation state threshold [17,37,41,47]. We did not observe this process across our higher temperature or salinity groups (Figure 4 – 6; SM. 5 – 7) however, we cannot definitively say that this absence is exclusive to low salinity environments. Kinetics likely play an increasing role at higher temperatures and salinities,

limiting the window for direct observation beyond the frequency of sampling in this study. Limited solid samples due to tank volume limitations and available resources for analysis constrained characterization. Further SEM and EDS samples at a finer time resolution, especially in early stages following alkalinity addition, would clarify salinity impacts on mineral formation.

By t_{48}, precipitated brucite in the S = 6.5 and 12.5 groups was fully replaced by aragonite (Figure 4 – 6). Newly formed aragonite was structurally different than that formed across temperature groups, with long, needle-like and rhombohedral structures coming from a central body (Figure 4), consistent with other aragonite precipitation studies [37,58,59]. Lower temperatures and slower precipitation kinetics during the critical mineral formation period likely yielded more ordered crystals at S= 6.5 and 12.5 groups (Figure 4), but SEM data were insufficient to assess morphology at other salinities (SM. 3). While we did not see a peak for brucite at S = 18.5, it is possible that this transition happened earlier than the t_3 sampling. No precipitate samples were collected for the T = 7.5°C group due to minimal visual precipitation in the tank until it was drained, at which point scant deposits of precipitate were observed on tank wall that was not sufficient for sample collection (SM. 3). Future work should prioritize larger tank volumes for filtration and solid collection. We note that when there is a lag time or extended induction time before precipitation becomes apparent through changes in seawater carbonate chemistry, turbidity, or visual whitening, it is very difficult to capture and quantify solid formation. We generally assume that this results in negligible loss of alkalinity from solution, particularly in open settings where the alkalinity-enhanced seawater is diluted and only begin accounting for precipitation mass and rate when it becomes experimentally feasible to do so. Because sampling for both solid and aqueous chemistry is destructive, significant scaling of time series contained

experiments towards mesocosms or field trials scale experiments would provide a more realistic step towards capturing relevant precipitation dynamics.

4.2 Application to OAE

Solid alkaline products may have lower precipitations thresholds since they inherently introduce nucleation sites that can significantly lower energy for mineral formation[40,41,58,60-62]. It is important to note that the thresholds found in our study, and those from Ringham, et al. [12], were derived using NaOH as a base product and may differ for other feedstocks. Alkaline feedstocks that directly alter the DIC pool, i.e. through the addition of CO_3^{2-} ions, may yield higher thresholds for alkaline stability due to their impact on both TA and DIC [16,18]. Beyond feedstock type (i.e., NaOH, carbonate minerals, hydroxides, or other sources) and the immediate impact on Ω_{ar}, the method of distribution (i.e., coastal outfalls, patch distribution, seabed placement, or other modes) and the phase of distribution (i.e., liquid, slurry, solid) will strongly influence secondary precipitation potential. Precipitation becomes highly dependent on spatial dynamics where alkalinity is distributed by coastal outfalls that are intended to rapidly dilute the source. Alkaline feedstocks that introduce nucleation sites demand careful dissolution accounting to avoid overestimating CO_2 uptake or promoting further precipitation. This necessitates further refinement to represent both induction times required for carbonate precipitation under varying chemical and environmental factors, and precipitation of other minerals such as brucite that may precede carbonate precipitation in seawater, altering in-water carbonate chemistry and potentially providing nucleation surfaces (if it does not rapidly redissolve due to outfall momentum and other factors). Ultimately, further research on the effects of temperature, salinity, carbonate chemistry, suspended nuclei, and alkaline distribution phase and mode are needed to determine

563 both reasonable operating thresholds to limit secondary precipitation, and to develop engineering
564 methods to quantify, mitigate, or avoid precipitation during an OAE deployment. Such methods
565 to limit precipitation during an OAE project may include deployment design that promotes rapid
566 dilution of alkalinity into the ocean or adjusts effluent hardness to preferentially promote or
567 avoid precipitation of specific minerals in seawater (Ebb Carbon, 2026).

568 Including secondary precipitation dynamics is essential for accurate OAE carbon
569 accounting. This study provides an opportunity to consider how precipitation dynamics may be
570 considered for project development and suggests that it may be challenging to initiate
571 precipitation at realistic alkalinity release levels within regional-scale models. Simulated effects
572 of secondary precipitation are highly sensitive to temperature and salinity, as observed by large
573 TA differences across seasons and spatial scales both in absolute values and percentages, and
574 warrant further experimentation across the range of possible coastal conditions (Figure 7 – 8;
575 SM. 8 – 19). However, the amount of alkalinity necessary to trigger and test secondary
576 precipitation dynamics within the reasonably fine spatial resolution regional model configuration
577 utilized here is exceedingly large and likely techno-economically infeasible. The necessary
578 alkalinity addition to trigger precipitation is also unrealistic for both regulatory and
579 environmental safety metrics, resulting in a large spatial patch of seawater that is significantly
580 elevated in alkalinity such that we would also expect significant changes in pH, pCO_2, and other
581 chemical parameters. For our model simulation, we released 4.05 mmol m^{-2} s^{-1} of alkalinity to
582 reach sufficiently high Ω_{ar} to trigger precipitation that were not immediately diluted by physical
583 mixing. Testing the same type of precipitation module and logic at a much finer resolution
584 capable of capturing high Ω_{ar} within a realistic OAE project is necessary for further
585 development, with the caveat that not all OAE simulations will drive significant saturation states

586 relative to precipitation. Within a previous study on electrochemical OAE in Sequim Bay[10],
587 simulations of alkalinity release were based on the Ebb Carbon pilot and at 1000x scale,
588 representing a realistic discharge of 1.75 $m^3 s^{-1}$, similar to large municipal or industrial
589 wastewater plants in the region. These alkalinity additions represented at maximum 164 Mmol of
590 TA added through a coastal outfall and held at pH 9, which is dissimilar to the patch of alkalinity
591 distributed into the ROMS grid used in this study. The resulting Ω_{ar} values were $\leq$6 within
592 Sequim Bay, far below relevant precipitation thresholds, so a precipitation module as described
593 in this study would not have been significant, even at the fine scale of the outfall that the Salish
594 Sea Model was used to represent. Laurent, et al. [46] and Ho, et al. [63] both used finer horizontal
595 resolutions (50 and 60 m, respectively), but simulated alkalinity release at pH < 9, avoiding
596 consideration of secondary precipitation. Heede, et al. [64] also used a fine nested grid (50 m) but
597 applied a small enough alkalinity forcing to avoid precipitation, and Anderson, et al. [65] (200 m)
598 also avoided releasing alkalinity above relevant precipitation thresholds. While these studies
599 have collectively avoided the need to quantify precipitation by setting bounds on alkalinity
600 release, there is significant interest in OAE scaling that bridges into scenarios where precipitation
601 becomes more relevant. OAE deployments using $Ca(OH)_2$, NaOH, and other alkaline products
602 that can rapidly supersaturate carbonate locally must evaluate how to effectively result in net
603 carbon removal at scale, which could rely on appropriate dilution as mentioned above, rather
604 than remaining below precipitation thresholds that limit total alkaline discharge. Recent field
605 deployments have tested this approach: the LOC-NESS release of 50 wt% NaOH into the Gulf of
606 Maine (MPRSA Research Permit EPA-HQ-MRPSA-2024-002, April 2025) and Ebb Carbon's
607 Project Macoma, which included permitted release of electrochemically generated alkalinity into
608 Port Angeles Harbor, WA, USA, with pH limits of 9.8 and 12.0[24] (Ebb Carbon, 2026; WA

609 NPDES Permit WA0991051). Both studies generated secondary precipitation during project
610 operations, making quantification and modeling of alkalinity loss a priority for future work,
611 particularly in the design of mitigation actions as OAE scales. Integrating experimentally-derived
612 secondary precipitation dynamics within near-field models, which could include dilution models
613 such as PLUMES2.0 used in predicting effluent transport, finer-scale nested Regional Ocean
614 Modeling System, or unstructured Finite Volume Community Ocean Models, therefore becomes
615 useful to characterize potential losses of inorganic carbon and alkalinity from the system,
616 bridging the gap in scale between near-field and regional models such as is relevant for accurate
617 carbon crediting (Cross et al. *in review*).

618

619 *4.3 Recommendations for future work*

620 Insights gained from this study could be further improved by addressing some of its
621 limitations. First, tank volume constrained space for sensor deployment and the frequency of
622 destructive sampling; larger tanks would allow finer temporal resolution after alkalinity addition,
623 which is particularly relevant in considering the distribution and rapid dilution of alkalinity into
624 seawater during scaled field tests. Second, discrete pH or pCO_2 samples may resolve carbonate
625 chemistry better than DIC, which responds much slower to carbon uptake. Third, rapid sample
626 analysis is as critical as collection: even filtered bottle samples risk precipitation while queued
627 for TA and DIC titrations. Precipitation can bias measurements both by further precipitating
628 alkalinity out of solution over time, and altering measurements where that precipitate is acidified
629 during titrations. Throughout this experiment, samples were not analyzed if there were visible
630 solid precipitates, however, mineral formation below visual detection is a risk in these analyses.
631 Finally, most treatments across the study did not trigger detectable precipitation as indicated by

visual observations, turbidity measurements, aqueous carbonate samples, or solid samples, such that any precipitation that may have occurred was not detected and deemed insignificant. Where precipitation was evident, we lacked an efficient method to separate and collect the bulk solids, which could be used to quantify total alkalinity lost from solution, beyond extrapolating rates of precipitation to the seawater volume. Whether these results hold with scale is important to OAE field deployments, which can consider laboratory assessments of relevant precipitation thresholds and stress test both additional parameters and additional monitoring methods in situ. Future threshold studies could explore temperature- salinity covariance, impacts of suspended particulates, and presence of biological communities, all of which would useful in interpreting field data. Iterative testing of precipitation thresholds, rates, and characterization across field and model applications will reduce uncertainty in precipitation-related alkalinity loss during OAE deployments, improving assessments of gross CDR.

This study demonstrated a process of determining conservative Ω_{ar} thresholds relevant for NaOH addition across salinity and temperature gradients relevant to many coastal environments. We emphasize that these thresholds do not represent biological thresholds for safe operation but instead operational limits for optimizing OAE delivery and minimizing secondary precipitation. The experiments were intentionally designed to inform model parameterization; combined with literature values, they predict alkalinity loss in a scaled regional model and highlight the need to represent precipitation reaction pathways in regional ocean model predictions of OAE efficiency and gross CDR from mCDR experiments. Continued refinements and data collection will support future OAE design, operation, and deployment. We hope these data will serve as a valuable resource to the broader OAE community and spark further investigation to improve climate change mitigation tools.

655 **Figure Captions**

656 *Figure 1*. **Logical flow diagram of experimental design and precipitation module inputs**.

657

658 *Figure 2*. **Carbonate chemistry over time for each tank during the five temperature groups.**
659 Temperature (°C) impacts on total alkalinity (TA; µmol kg^{-1}, *top row, A – E*), dissolved inorganic
660 carbon (DIC; µmol kg^{-1}, *middle row, F – J*), and Ω_{ar} *(bottom row, K – O).* Temperature groups
661 increase from left to right (7.5, 11, 16, 21, 29.5 ˚C). Data includes both filtered (*dashed, open*
662 *symbols*) and unfiltered seawater (*solid, closed symbols*), with darker colors indicating higher
663 alkalinity treatments for both groups. Alkalinity treatments are identified as control (+0 µmol kg^{-1}, *circles*), +1500 µmol kg^{-1} (*triangles*), +2500 µmol kg^{-1} (*squares*), and +3500 µmol kg^{-1}
665 (*diamonds*).

666

667 *Figure 3*. **Carbonate chemistry over time for each tank during the five salinity groups.**
668 Salinity impacts on total alkalinity (TA; µmol kg^{-1}, *top row, A – E*), dissolved inorganic carbon
669 (DIC; µmol kg^{-1}, *middle row, F – J*), and Ω_{ar}, *bottom row, K – O).* Salinity groups increase from
670 left to right (6.5, 12.5, 18.5, 24.5, and 32.5). Data includes both filtered (*dashed, open symbols*)
671 and unfiltered seawater (*solid, closed symbols*), with darker colors indicating higher alkalinity
672 treatments for both groups. Alkalinity treatments are identified as control (+0 µmol kg^{-1}, *circles*),
673 +1500 µmol kg^{-1} (*triangles*), +2500 µmol kg^{-1} (*squares*), and +3500 µmol kg^{-1} (*diamonds*).

674

675 *Figure 4*. **XRD spectra of precipitated minerals from experiment 1 and 2.** XRD spectra of
676 samples taken from the +3500 µmol kg^{-1} treatment from filtered (blue, dashed lines) and
677 unfiltered (pink, solid lines) tanks. Experiment 1 data (left) are from the T = 29.5 °C group and
678 experiment 2 data (right) are from the S = 6.5 salinity. Samples are from t_3 (lightest colors), t_{24},
679 and t_{48} hours (darkest colors) after base addition. Reference spectra are on the bottom of each
680 XRD for brucite (Desgranges, et al. [66]) aragonite (Jarosch and Heger [67]), and calcite (Caspi, et al.
681 [68]).

682

683 *Figure 5*. **SEM results of solid precipitate samples collected over time during experiment 1**
684 **and 2.** All data are from high alkalinity (±3500 µmol kg^{-1}) treatment filtered tanks. (Left) SEM
685 photos of precipitate samples collected from Experiment 1 during the T = 30°C group. (Right)
686 SEM photos of precipitate samples collected from Experiment 2 during the S = 6.5 group. Time
687 increases from top to bottom where (A & B) are 3 hours, (C & D) are 24 hours, and (E & F) are
688 48 hours after base addition. All images are at the 30 µm scale.

689

690 *Figure 6*. **EDS mapping results of solid precipitate samples collected over time during each**
691 **experiment.** All data are from high alkalinity (±3500 µmol kg^{-1}) treatment tanks. (Top row)
692 Composition of precipitate samples collected from Experiment 1 during the T = 30°C group.
693 (Middle row) Bar chart of atomic percentage of Ca and Mg of each analyzed precipitate sample
694 normalized to 100% with sample description and percent values below each bar. (Bottom row)
695 Composition of precipitate samples collected from Experiment 2 during the S = 6.5 group. Time
696 increases from left to right. EDS maps (20 µm scale) of the analyzed sample are color coding

based on elements present, where Mg is red and Ca is blue. Data from both filtered and unfiltered (*UF) tanks are included at t_{24}.

Figure 7. **Time-series responses of surface alkalinity (meq m^{-3}) with and without the precipitation module averaged over the plume**. Simulations run with the precipitation module enabled (dashed line) and no module (solid line) during (A) January and (B) June. Oligohaline releases of alkalinity in Baltimore Harbor are shown in red while southern mesohaline Bay releases are shown in blue.

Figure 8. **Monthly-averaged surface alkalinity responses to the representation of secondary precipitation dynamics**. The difference in alkalinity is representative of the change due to secondary precipitation alone during (A-B) January and (C-D) June for the (A & C) Baltimore Harbor release site and (B & D) Southern Bay release site. Release point is shown with the red arrow on panels A & B.

Acknowledgements

We would like to thank team members Marjorie A. M. Friedrichs, Pierre St-Laurent, Claudine Hauri, Parker MacCready, and Aurora Leeson who helped conceptualize the modeling work. The author(s) declare that financial support was received for the research and/or publication of this article. This study was led by Pacific Northwest National Laboratory, which is operated for the US Department of Energy by Battelle Memorial Institute under contract DE-AC05-76RL01830. Financial support for the research was provided by the US Department of Energy's Advanced Research Projects Agency – Energy (ARPA-E) (Project #22/CJ000/09/08). Support for ES was

719 provided by the Department of Energy, Science Undergraduate Laboratory Internships (SULI)
720 program. Production of the alkaline feedstock was carried out by Ebb Carbon, which also
721 financially supported MR. We thank Tyson Minck, Jeremy Loretz, and Todd Pelman from Ebb
722 Carbon for contributions to this work. We thank Cody Shaw from Stony Brook University for
723 discussions on methodology. Part of this work was conducted at the Molecular Analysis Facility,
724 a National Nanotechnology Coordinated Infrastructure (NNCI) site at the University of
725 Washington, which is supported in part by funds from the National Science Foundation (awards
726 NNCI-2025489, NNCI-1542101), the Molecular Engineering & Sciences Institute, and the Clean
727 Energy Institute.

728

729 **Author Contributions**

730 AMS – conceptualization, methodology, validation, formal analysis, investigation, data curation,
731 writing – original draft, writing – review & editing, visualization. KH – methodology, software,
732 formal analysis, investigation, writing – original draft, writing – review & editing, visualization.
733 AB – formal analysis, investigation, writing – original draft, writing – review & editing,
734 visualization. MR – conceptualization, methodology, resources, writing – review & editing. ES –
735 data curation, investigation, writing – review & editing. CS- conceptualization, resources,
736 writing – review & editing, supervision. JC – supervision, conceptualization, writing – review &
737 editing. RP – methodology, validation, writing – review & editing. AKL – methodology,
738 validation, writing – review & editing. JX – validation, writing – review & editing. ZY-
739 conceptualization, resources, writing – review & editing, supervision, project administration,
740 funding acquisition. NW – conceptualization, methodology, resources, writing – review &
741 editing, supervision, project administration, funding acquisition.

Competing Interests

Author MR was employed by Ebb Carbon, Inc. The remaining authors declare that the research was conducted in the absence of any commercial or financial relationships that could be construed as a potential conflict of interest.

Data Availability Statement

Data has been included with the manuscript submission for reviewers/editors. It will be made openly available pending acceptance either through NOAA's NCEI or GitHub.

References

1 Rogelj, J. *et al.* Scenarios towards limiting global mean temperature increase below 1.5 °C. *Nature Climate Change* **8**, 325–332 (2018). https://doi.org/10.1038/s41558-018-0091-3

2 Fuhrman, J. *et al.* Diverse carbon dioxide removal approaches could reduce impacts on the energy–water–land system. *Nature Climate Change* **13**, 341–350 (2023). https://doi.org/10.1038/s41558-023-01604-9

3 IPCC. IPCC, 2023: Climate Change 2023: Synthesis Report. 35–115 (IPCC, Generva, Switzerland, 2023).

4 National Academies of Sciences, E., Medicine;. *A Research Strategy for Ocean-based Carbon Dioxide Removal and Sequestration*. (The National Academies Press, 2022).

5 Renforth, P. & Henderson, G. Assessing ocean alkalinity for carbon sequestration. *Reviews of Geophysics* **55**, 636–674 (2017). https://doi.org/10.1002/2016rg000533

6 Oschlies, A. *et al.* Climate targets, carbon dioxide removal, and the potential role of ocean alkalinity enhancement. *Guide to Best Practices in Ocean Alkalinity Enhancement Research* **2-oae2023**, 1 (2023). https://doi.org/10.5194/sp-2-oae2023-1-2023

7 Eisaman, M. D. *et al.* Assessing the technical aspects of ocean-alkalinity-enhancement approaches. *Guide to Best Practices in Ocean Alkalinity*

Enhancement Research **2-oae2023**, 3 (2023). https://doi.org/10.5194/sp-2-oae2023-3-2023

8 Savoie, A. M. *et al.* Novel field trial for ocean alkalinity enhancement using electrochemically derived aqueous alkalinity. *Frontiers in Environmental Engineering* **Volume 4 - 2025** (2025). https://doi.org/10.3389/fenve.2025.1641277

9 Eisaman, M. D. Pathways for marine carbon dioxide removal using electrochemical acid-base generation. *Frontiers in Climate* **Volume 6 - 2024** (2024). https://doi.org/10.3389/fclim.2024.1349604

10 Khangaonkar, T. *et al.* Mixing and dilution controls on marine CO2 removal using alkalinity enhancement. *Environmental Research Letters* **19** (2024). https://doi.org/10.1088/1748-9326/ad7521

11 La Plante, E. C. *et al.* Electrolytic Seawater Mineralization and the Mass Balances That Demonstrate Carbon Dioxide Removal. *ACS ES&T Engineering* **3**, 955–968 (2023). https://doi.org/10.1021/acsestengg.3c00004

12 Ringham, M. C. *et al.* An assessment of ocean alkalinity enhancement using aqueous hydroxides: kinetics, efficiency, and precipitation thresholds. *Biogeosciences* **21**, 3551–3570 (2024). https://doi.org/10.5194/bg-21-3551-2024

13 Ferderer, A., Chase, Z., Kennedy, F., Schulz, K. G. & Bach, L. T. Assessing the influence of ocean alkalinity enhancement on a coastal phytoplankton community. *Biogeosciences* **19**, 5375–5399 (2022). https://doi.org/10.5194/bg-19-5375-2022

14 Bach, L. T., Ferderer, A. J., LaRoche, J. & Schulz, K. G. Technical note: Ocean Alkalinity Enhancement Pelagic Impact Intercomparison Project (OAEPIIP). *Biogeosciences* **21**, 3665–3676 (2024). https://doi.org/10.5194/bg-21-3665-2024

15 Kousoulas, K., Ferderer, A., Eriksen, R. & Bach, L. T. Winners and losers under hydroxide-based ocean alkalinity enhancement in a Tasmanian plankton community. *Journal of Phycology* **9** (2025). https://doi.org/https://doi.org/10.1111/jpy.70052

16 Hartmann, J. *et al.* Stability of alkalinity in ocean alkalinity enhancement (OAE) approaches – consequences for durability of CO2 storage. *Biogeosciences* **20**, 781–802 (2023). https://doi.org/10.5194/bg-20-781-2023

17 Suitner, N. *et al.* Ocean alkalinity enhancement approaches and the predictability of runaway precipitation processes: results of an experimental study to determine critical alkalinity ranges for safe and sustainable application scenarios. *Biogeosciences* **21**, 4587–4604 (2024). https://doi.org/10.5194/bg-21-4587-2024

18 Suitner, N. *et al.* Surface area and Ω-aragonite oversaturation as controls of the runaway precipitation process in ocean alkalinity enhancement. *EGUsphere* **2025**, 1–26 (2025). https://doi.org/10.5194/egusphere-2025-381

19 Jones, K. *et al.* Biological response of eelgrass epifauna, Taylor's sea hare (Phyllaplysia taylori) and eelgrass isopod (Idotea resecata), to elevated ocean alkalinity. *EGUsphere* **2024**, 1–25 (2024). https://doi.org/10.5194/egusphere-2024-972

20 Fucich, D., Lynch, H. J., Shaw, C., Eisaman, M. D. & Ringham, M. C. Determining the net influence of biological processes on aqueous hydroxide-based ocean alkalinity

enhancement: a mesocosm approach. *Frontiers in Climate* **Volume 7 - 2025** (2025). https://doi.org/10.3389/fclim.2025.1652680

21 Antoni, D., Wichels, A., Boersma, M. & Gerdts, G. The effect of ocean alkalinity enhancement on pelagic bacterial communities: focus points derived from a mesocosm experiment. *Frontiers in Microbiomes* **Volume 4 - 2025** (2025). https://doi.org/10.3389/frmbi.2025.1606890

22 Kittu, L. & Riebesell, U. Report on data of ocean alkalinization mesocosm experiment in a temperate zone neritic system. 20 (Kiel, Germany, 2025).

23 Goldenberg, S. U. *et al.* Early life stages of fish under ocean alkalinity enhancement in coastal plankton communities. *Biogeosciences* **21**, 4521–4532 (2024). https://doi.org/10.5194/bg-21-4521-2024

24 Ringham, M. C. *et al.* A novel methodology to characterize the potential impacts of electrochemical ocean alkalinity enhancement on juvenile coho salmon (Oncorhynchus kisutch). *Frontiers in Climate* **Volume 7 - 2025** (2026). https://doi.org/10.3389/fclim.2025.1717924

25 Albright, R. *et al.* Reversal of ocean acidification enhances net coral reef calcification. *Nature* **531**, 362–365 (2016). https://doi.org/10.1038/nature17155

26 Subhas, A. *et al.* in *Ocean Sciences Meeting*.

27 Wynn-Edwards, C. A. *et al.* Alkalinity enhancement with sodium hydroxide in coastal ocean waters. *Scientific Reports* **16**, 1842 (2025). https://doi.org/10.1038/s41598-025-31606-w

28 Ebb Carbon. (2026).

29 Wang, H. *et al.* Simulated Impact of Ocean Alkalinity Enhancement on Atmospheric CO2 Removal in the Bering Sea. *Earth's Future* **11** (2023). https://doi.org/10.1029/2022ef002816

30 He, J. & Tyka, M. D. Limits and CO2equilibration of near-coast alkalinity enhancement. *Biogeosciences* **20**, 27–43 (2023). https://doi.org/10.5194/bg-20-27-2023

31 Zhou, M. *et al.* Mapping the global variation in the efficiency of ocean alkalinity enhancement for carbon dioxide removal. *Nature Climate Change* **15**, 59–65 (2025). https://doi.org/10.1038/s41558-024-02179-9

32 Jones, D. C., Ito, T., Takano, Y. & Hsu, W. C. Spatial and seasonal variability of the air-sea equilibration timescale of carbon dioxide. *Global Biogeochemical Cycles* **28**, 1163–1178 (2014). https://doi.org/10.1002/2014gb004813

33 Bach, L. T., Ho, D. T., Boyd, P. W. & Tyka, M. D. Toward a consensus framework to evaluate air–sea CO2 equilibration for marine CO2 removal. *Limnology and Oceanography Letters* **8**, 685–691 (2023). https://doi.org/10.1002/lol2.10330

34 Mendes, I., Lübbers, J., Schönfeld, J. & Cravo, A. Evaluating ocean alkalinity enhancement for carbon dioxide removal: evidence from a one-year saltmarsh field experiment. *EGUsphere* **2025**, 1–25 (2025). https://doi.org/10.5194/egusphere-2025-4555

35 Zhong, S. & Mucci, A. Calcite and aragonite precipitation from seawater solutions of various salinities: Precipitation rates and overgrowth compositions. *Chemical*

Geology **78**, 283–299 (1989). https://doi.org/https://doi.org/10.1016/0009-2541(89)90064-8

36 Morse, J. W., Gledhill, D. K. & Millero, F. J. Caco3 precipitation kinetics in waters from the great Bahama bank:: Implications for the relationship between bank hydrochemistry and whitings. *Geochimica et Cosmochimica Acta* **67**, 2819–2826 (2003). https://doi.org/https://doi.org/10.1016/S0016-7037(03)00103-0

37 Moras, C. A., Saez Moreno, M., Bartsch, P. & Hartmann, J. Impacts of water advection and CO2 exchanges on the carbon dioxide removal potential of ocean alkalinity enhancement. *EGUsphere* **2026**, 1–28 (2026). https://doi.org/10.5194/egusphere-2025-6144

38 Berner, R. A., Lasaga, A. C. & Garrels, R. M. Carbonate-silicate geochemical cycle and its effect on atmospheric carbon dioxide over the past 100 million years. *Am. J. Sci.; (United States)* **283:7** (1983). https://doi.org/10.2475/ajs.283.7.641

39 Mucci, A. The solubility of calcite and aragonite in seawater at various salinities, temperatures, and one atmosphere total pressure. *American Journal of Science* **283**, 780–799 (1983). https://doi.org/10.2475/ajs.283.7.780

40 Schulz, K. G., Bach, L. T. & Dickson, A. G. Seawater carbonate chemistry considerations for ocean alkalinity enhancement research: theory, measurements, and calculations. *Guide to Best Practices in Ocean Alkalinity Enhancement Research* **2-oae2023**, 2 (2023). https://doi.org/10.5194/sp-2-oae2023-2-2023

41 Morse, J. W., Arvidson, R. S. & Lüttge, A. Calcium carbonate formation and dissolution. *Chemical reviews* **107 2**, 342–381 (2007).

42 Wurgaft, E., Steiner, Z., Luz, B. & Lazar, B. Evidence for inorganic precipitation of CaCO3 on suspended solids in the open water of the Red Sea. *Marine Chemistry* **186**, 145–155 (2016). https://doi.org/https://doi.org/10.1016/j.marchem.2016.09.006

43 Fennel, K. *et al.* Modelling considerations for research on ocean alkalinity enhancement (OAE). *Guide to Best Practices in Ocean Alkalinity Enhancement Research* **2-oae2023**, 9 (2023). https://doi.org/10.5194/sp-2-oae2023-9-2023

44 Ward, N. D. *et al.* Regional ocean biogeochemical modeling challenges for predicting the effectiveness of marine carbon dioxide removal. *Frontiers in Climate* **Volume 7 - 2025** (2025).

45 Suselj, K. *et al.* Quantifying Marine Carbon Dioxide Removal via Alkalinity Enhancement Across Circulation Regimes Using ECCO-Darwin and 1D Models. *Journal of Advances in Modeling Earth Systems* **17**, e2024MS004847 (2025). https://doi.org/https://doi.org/10.1029/2024MS004847

46 Laurent *et al.* A high-resolution nested model to study the effects of alkalinity additions in Halifax Harbour, a mid-latitude coastal fjord. *EGUsphere* **2025**, 1–37 (2025). https://doi.org/10.5194/egusphere-2025-3361

47 Hashim, M. *et al.* Mineral Formation during Shipboard Ocean Alkalinity Enhancement Experiments in the North Atlantic. *EGUsphere* **2025**, 1–31 (2025). https://doi.org/10.5194/egusphere-2025-988

48 Dickson, A. G., Sabine, C. L. & Christian, J. R. Guide to Best Practices for Ocean CO2 Measurements. *PICES Special Publication* **3**, 191 (2007).

49 Millero, F. Carbonate constants for estuarine waters. *Marine and Freshwater Research* **61**, 139–142 (2010). https://doi.org/10.1071/MF09254

50 Dickson, A. G. Standard potential of the reaction: AgCl(s) + 12H2(g) = Ag(s) + HCl(aq), and and the standard acidity constant of the ion HSO4− in synthetic sea water from 273.15 to 318.15 K. *The Journal of Chemical Thermodynamics* **22**, 113–127 (1990). https://doi.org/https://doi.org/10.1016/0021-9614(90)90074-Z

51 Perez, F. F. & Fraga, F. The pH measurements in seawater on the NBS scale. *Marine Chemistry* **21**, 315–327 (1987). https://doi.org/https://doi.org/10.1016/0304-4203(87)90054-5

52 Lee, K. *et al*. The universal ratio of boron to chlorinity for the North Pacific and North Atlantic oceans. *Geochimica et Cosmochimica Acta* **74**, 1801–1811 (2010). https://doi.org/https://doi.org/10.1016/j.gca.2009.12.027

53 St-Laurent, P. & Friedrichs, M. A. M. On the Sensitivity of Coastal Hypoxia to Its External Physical Forcings. *Journal of Advances in Modeling Earth Systems* **16**, e2023MS003845 (2024). https://doi.org/https://doi.org/10.1029/2023MS003845

54 Li, M. *et al*. Wastewater alkalinity enhancement for carbon emission reduction and marine CO2 removal. *Environmental Research Letters* **20**, 044041 (2025). https://doi.org/10.1088/1748-9326/adc1e3

55 Bach, L. T. *et al*. An approach for particle sinking velocity measurements in the 3–400 µm size range and considerations on the effect of temperature on sinking rates. *Marine Biology* **159**, 1853–1864 (2012). https://doi.org/10.1007/s00227-012-1945-2

56 Lebrato, M. *et al*. Global variability in seawater Mg:Ca and Sr:Ca ratios in the modern ocean. *Proceedings of the National Academy of Sciences of the United States of America*, 201918943 (2020). https://doi.org/10.1073/pnas.1918943117

57 Pokrovsky, O. S. & Schott, J. Experimental study of brucite dissolution and precipitation in aqueous solutions: surface speciation and chemical affinity control. *Geochimica et Cosmochimica Acta* **68**, 31–45 (2004). https://doi.org/https://doi.org/10.1016/S0016-7037(03)00238-2

58 Moras, C. A., Bach, L. T., Cyronak, T., Joannes-Boyau, R. & Schulz, K. G. Ocean alkalinity enhancement – avoiding runaway CaCO3 precipitation during quick and hydrated lime dissolution. *Biogeosciences* **19**, 3537–3557 (2022). https://doi.org/10.5194/bg-19-3537-2022

59 Willinger, M.-G. *et al*. Structural evolution of aragonite superstructures obtained in the presence of the siderophore deferoxamine. *CrystEngComm* **17**, 3927–3935 (2015). https://doi.org/10.1039/C5CE00186B

60 Marion, G. M., Millero, F. J. & Feistel, R. Precipitation of solid phase calcium carbonates and their effect on application of seawater S_A–T–P models. *Ocean Sci.* **5**, 285–291 (2009). https://doi.org/10.5194/os-5-285-2009

61 Moras, C. A., Bach, L. T., Cyronak, T., Joannes-Boyau, R. & Schulz, K. G. Preparation and quality control of in-house reference materials for marine dissolved inorganic carbon and total alkalinity measurements. *Limnology and Oceanography: Methods* **21**, 637–644 (2023). https://doi.org/10.1002/lom3.10570

62 Sun, W., Jayaraman, S., Chen, W., Persson, K. A. & Ceder, G. Nucleation of metastable aragonite CaCO₃ in seawater. *Proceedings of the National Academy of Sciences* **112**, 3199–3204 (2015). https://doi.org/doi:10.1073/pnas.1423898112

63 Ho, M. *et al.* Ocean alkalinity enhancement in an estuary. *Frontiers in Climate* **Volume 7 - 2025** (2026). https://doi.org/10.3389/fclim.2025.1665329

64 Heede, U. K. *et al.* Simulating enhanced ocean alkalinity experiments in a high-latitude fjord using nested ROMS simulations coupled with MARBL biogeochemistry. *EGUsphere* **2026**, 1–32 (2026). https://doi.org/10.5194/egusphere-2026-2920

65 Anderson, H. J., Mongin, M. & Matear, R. J. Ocean alkalinity enhancement in a coastal channel: simulating localised dispersion, carbon sequestration and ecosystem impact. *Environmental Research Communications* **7**, 041012 (2025). https://doi.org/10.1088/2515-7620/adce5a

66 Desgranges, L., Calvarin, G. & Chevrier, G. Interlayer interactions in M(OH)2: a neutron diffraction study of Mg(OH)2. *Acta Crystallographica Section B* **52**, 82–86 (1996). https://doi.org/doi:10.1107/S0108768195008275

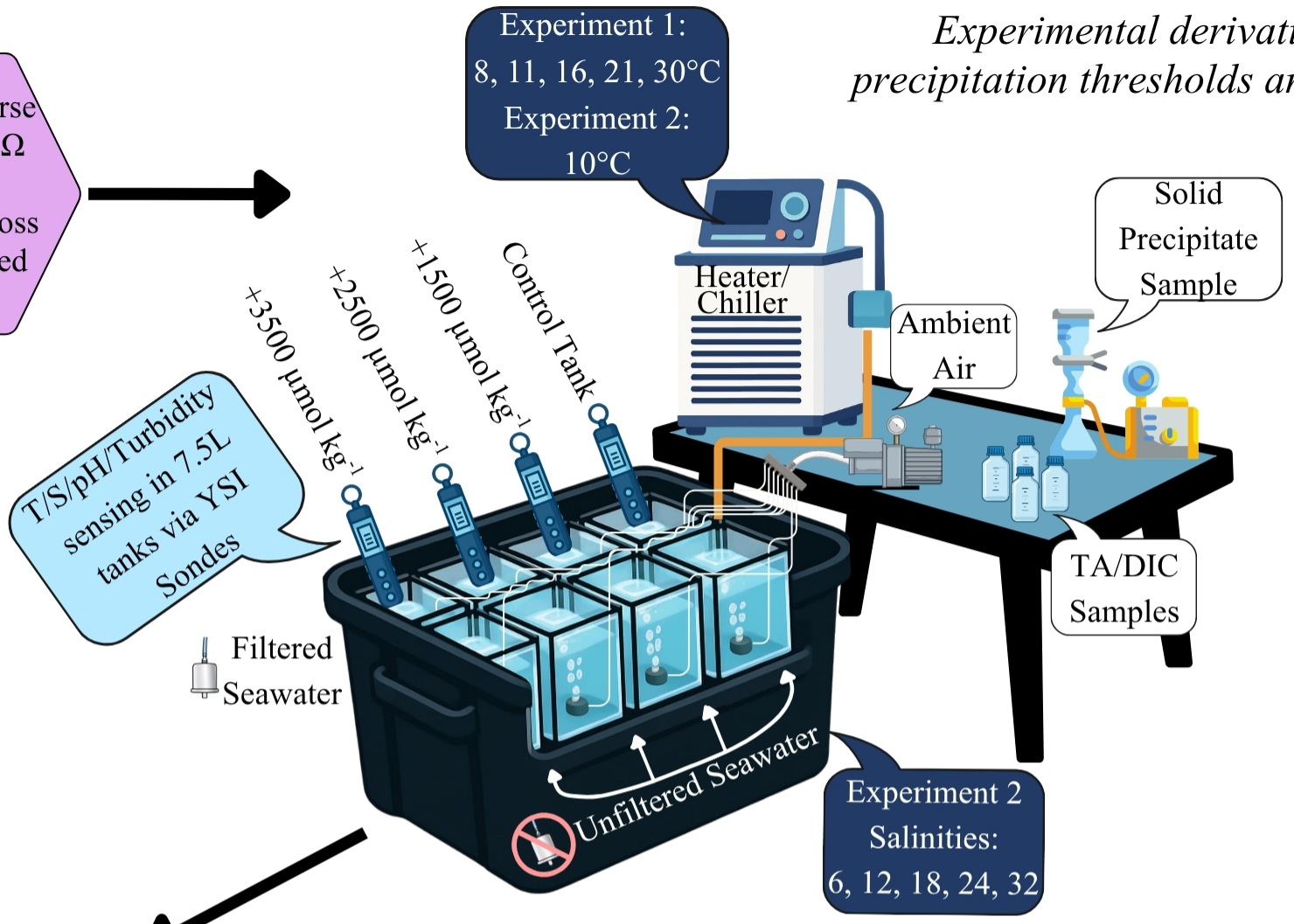
67 Jarosch, D. & Heger, G. Neutron diffraction refinement of the crystal structure of aragonite. *Tschermaks mineralogische und petrographische Mitteilungen* **35**, 127–131 (1986). https://doi.org/10.1007/BF01140844

68 Caspi, E. N., Pokroy, B., Lee, P. L., Quintana, J. P. & Zolotoyabko, E. On the structure of aragonite. *Acta Crystallographica Section B* **61**, 129–132 (2005). https://doi.org/doi:10.1107/S0108768105005240

Integrating secondary precipitation with OAE quantification

Motivation: Sparse data on critical Ω values for precipitation across T, S & suspended sediments

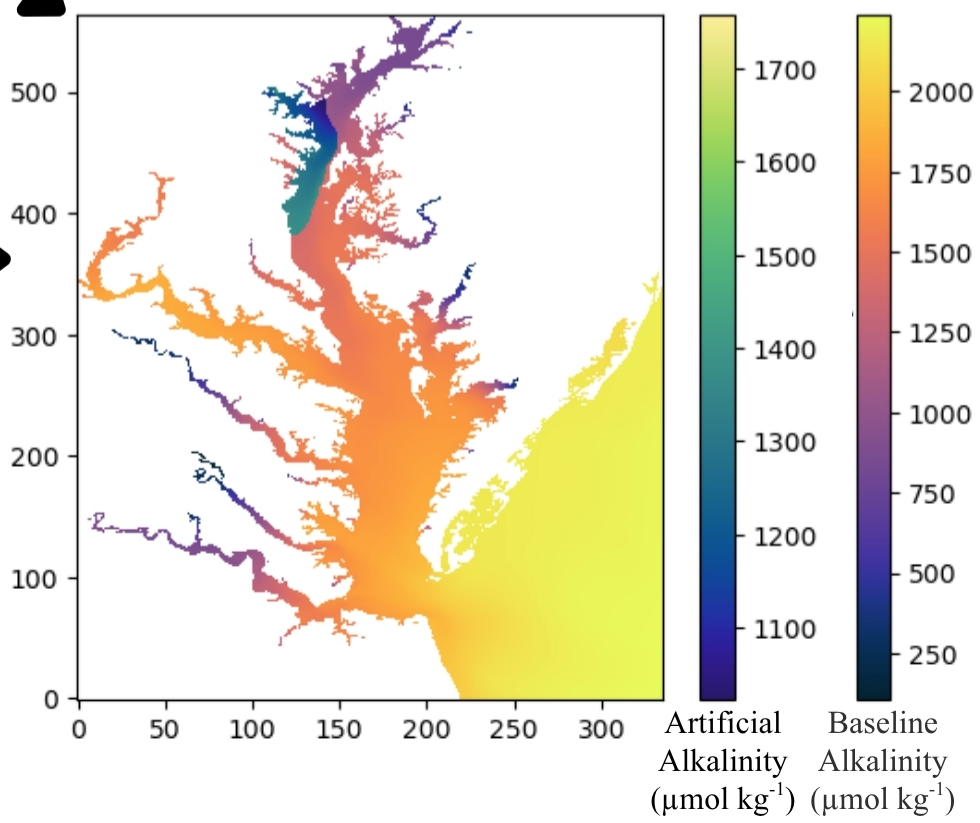
Experimental derivation of precipitation thresholds and kinetics



Experimentally derived logistical regression model to predict when precipitation may to occur @ a given T & S & Ω

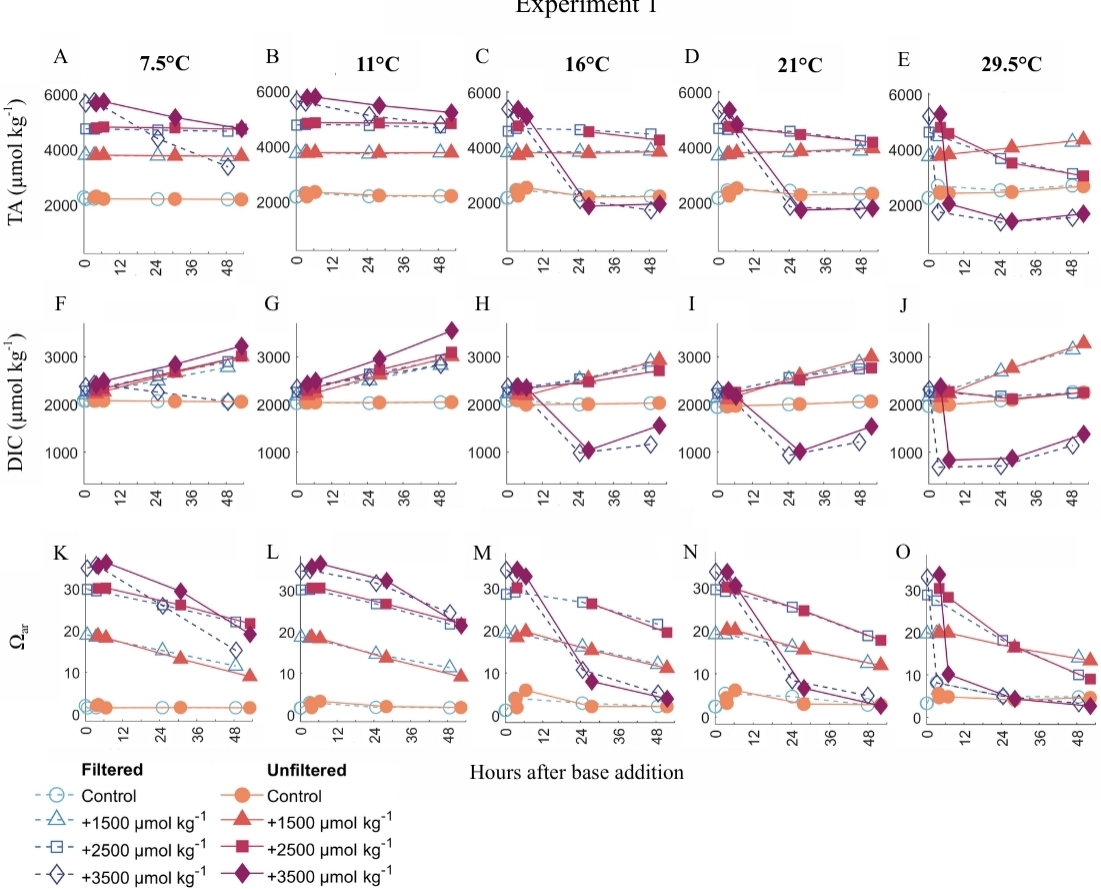
Incorporation of precipitation into regional OAE simulations

Precipitation Rate at a given Ω from previous research

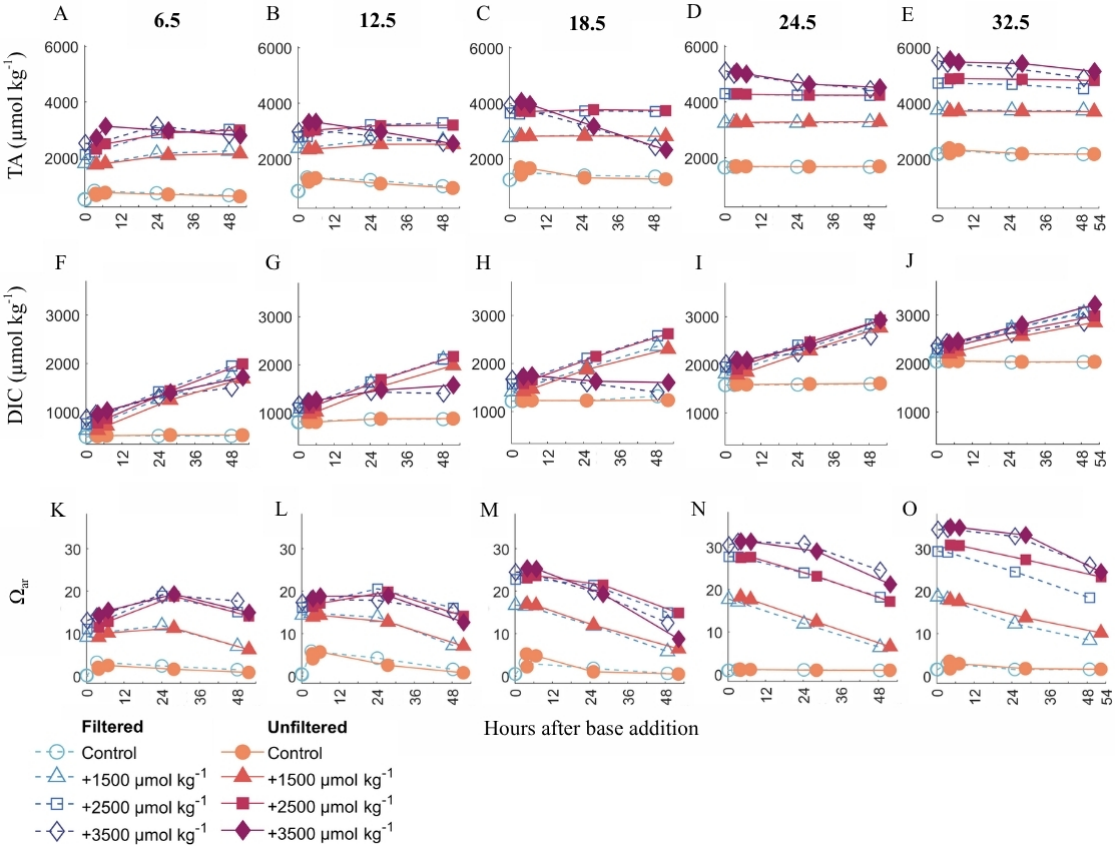


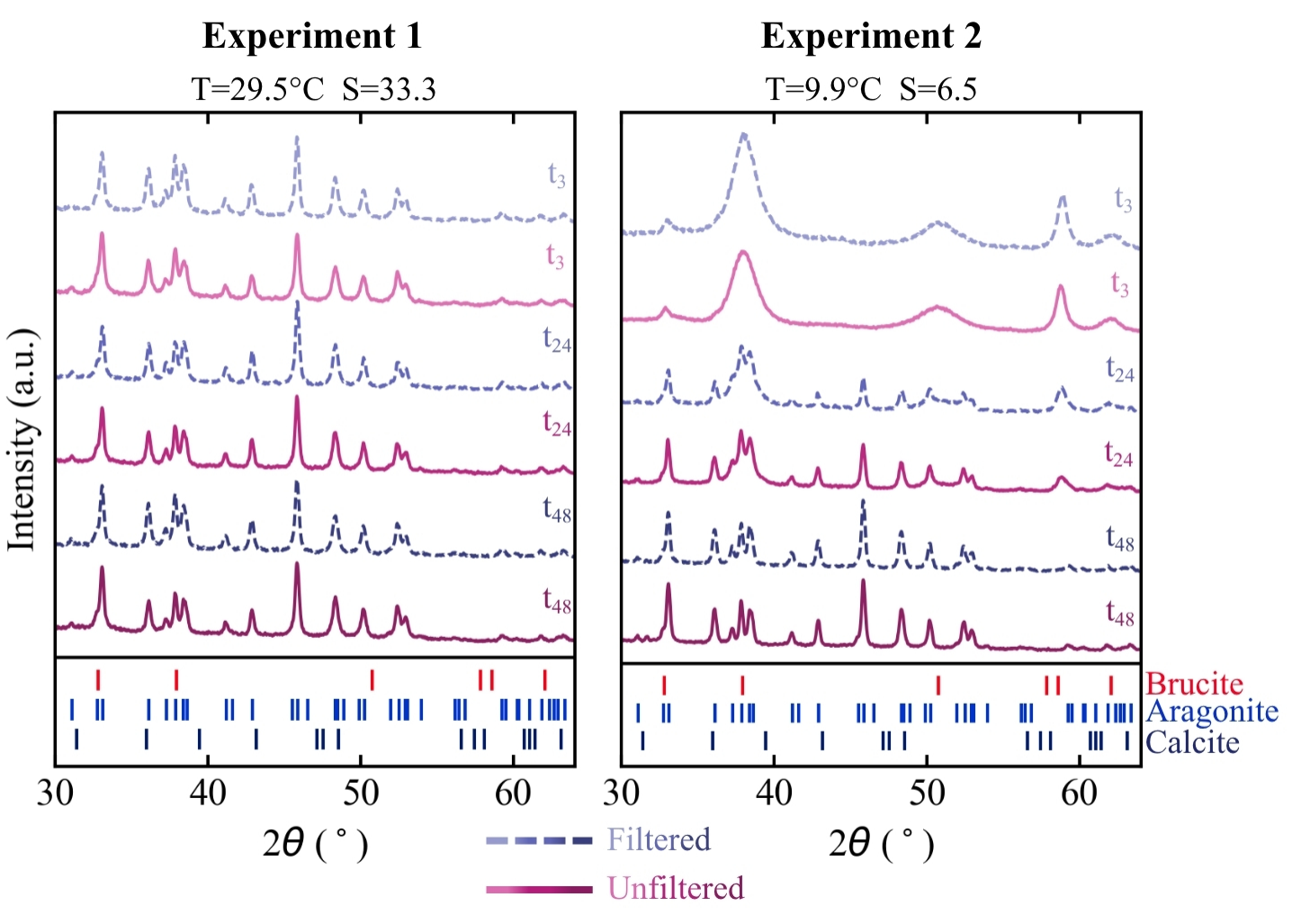
Iteration in lab, field, and model testing

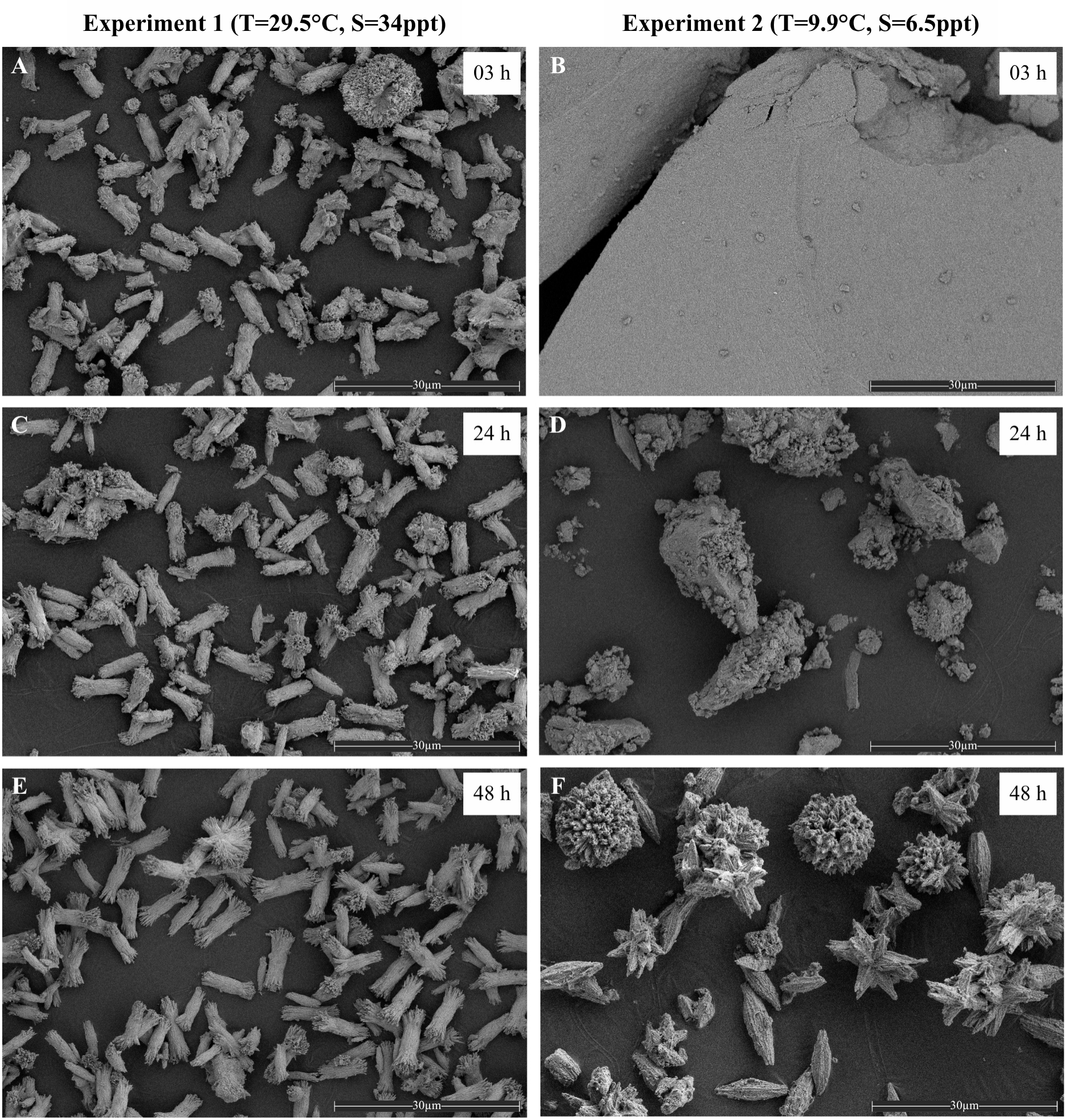
Use in OAE project design and assessments of alkaline delivery for CDR quantification

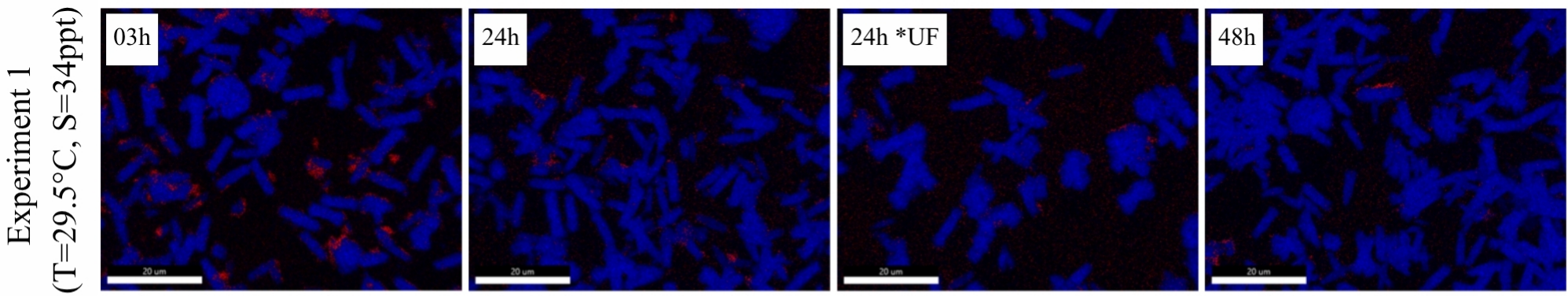

Experiment 1
A
7.5°C
B
11°C
C
16°C
D
21°C
E
29.5°C
TA (µmol kg-1)
DIC (µmol kg-1)
Ωar
F
G
H
I
J
K
L
M
N
O
Hours after base addition
Filtered
Control
+1500 µmol kg-1
+2500 µmol kg-1
+3500 µmol kg-1
Unfiltered
Control
+1500 µmol kg-1
+2500 µmol kg-1
+3500 µmol kg-1

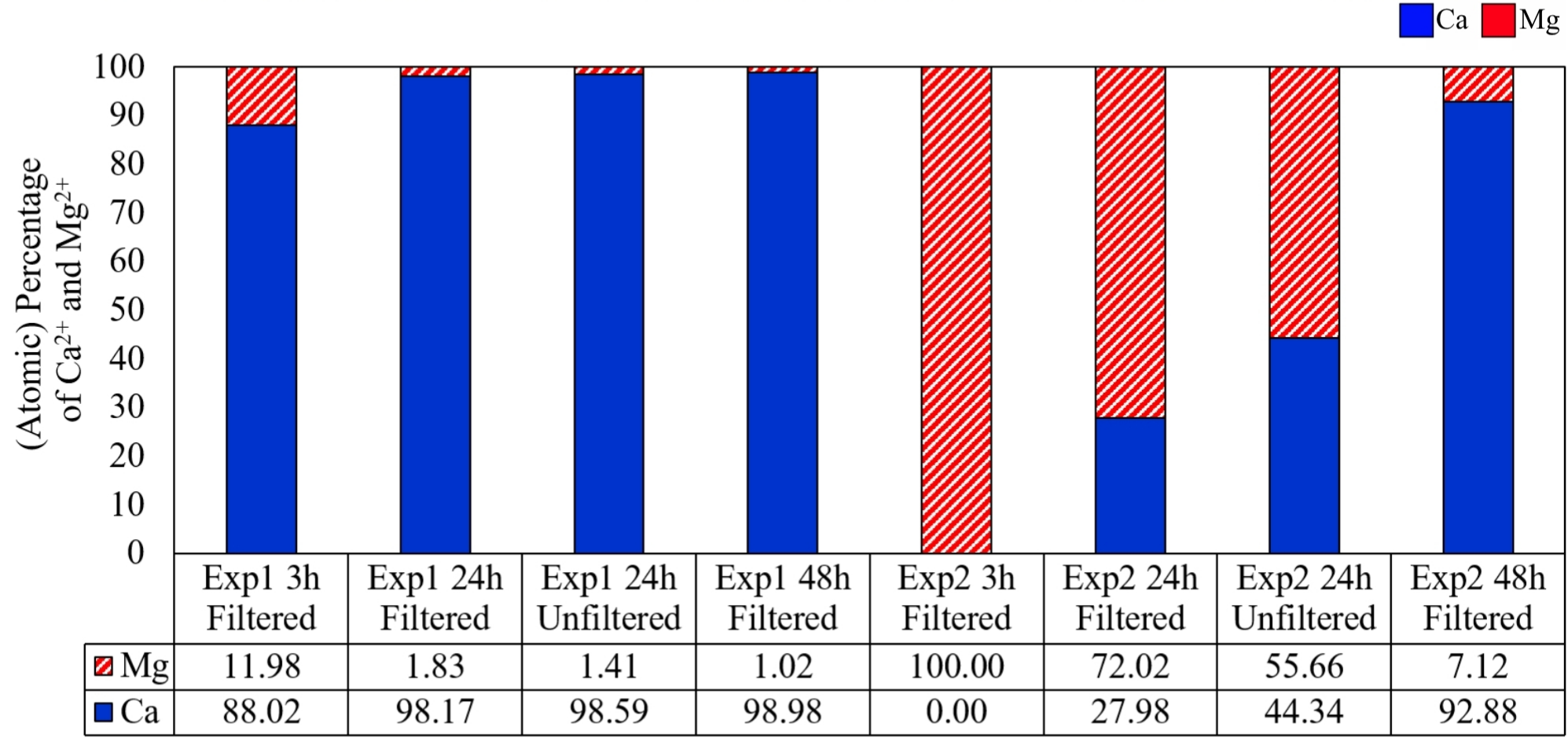
Experiment 2



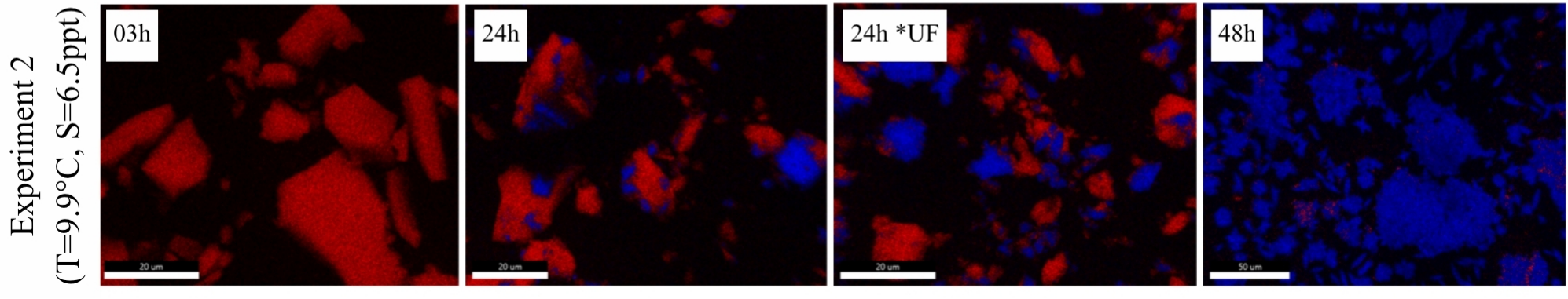

Experiment 1
T=29.5°C S=33.3
Experiment 2
T=9.9°C S=6.5
Intensity (a.u.)
t3
t3
t24
t24
t48
t48
Brucite
Aragonite
Calcite
30
40
50
60
2θ (°)
Filtered
Unfiltered

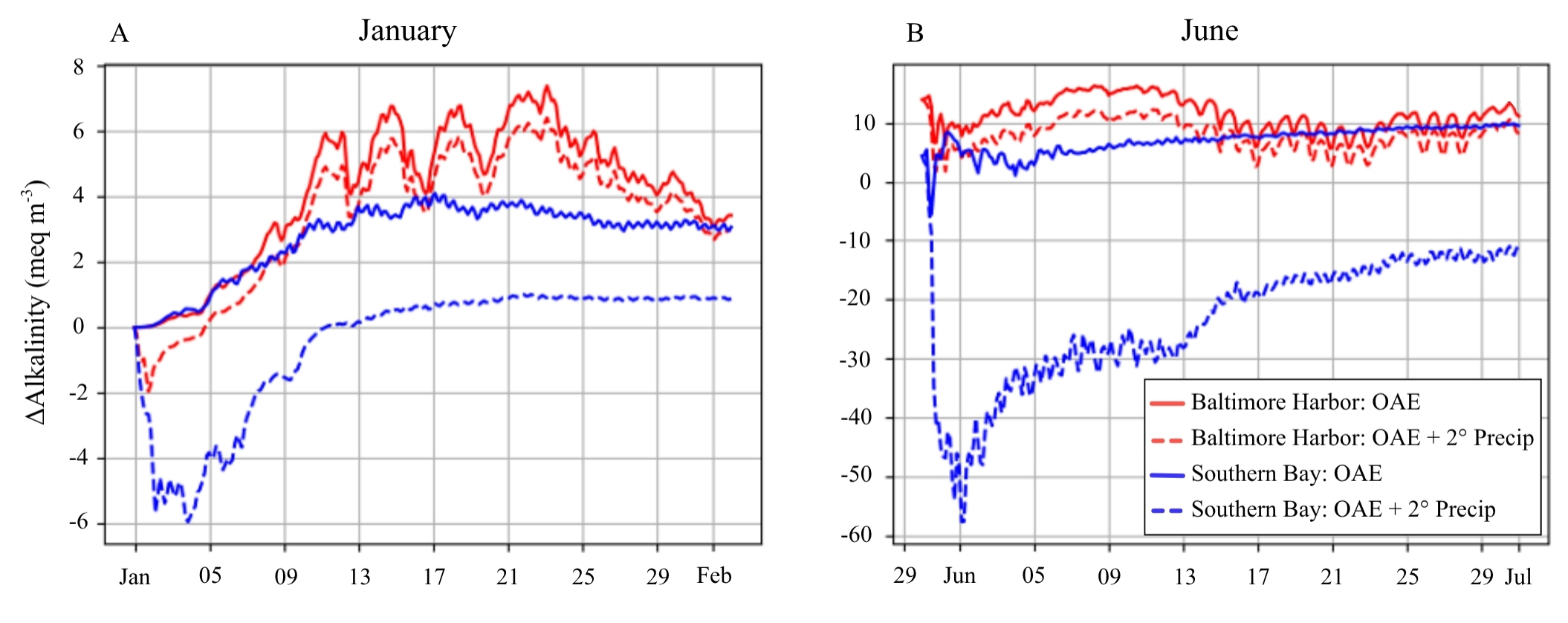

Experiment 1 (T=29.5°C, S=34ppt)
Experiment 2 (T=9.9°C, S=6.5ppt)
A
03 h
30µm
B
03 h
30µm
C
24 h
30µm
D
24 h
30µm
E
48 h
30µm
F
48 h
30µm

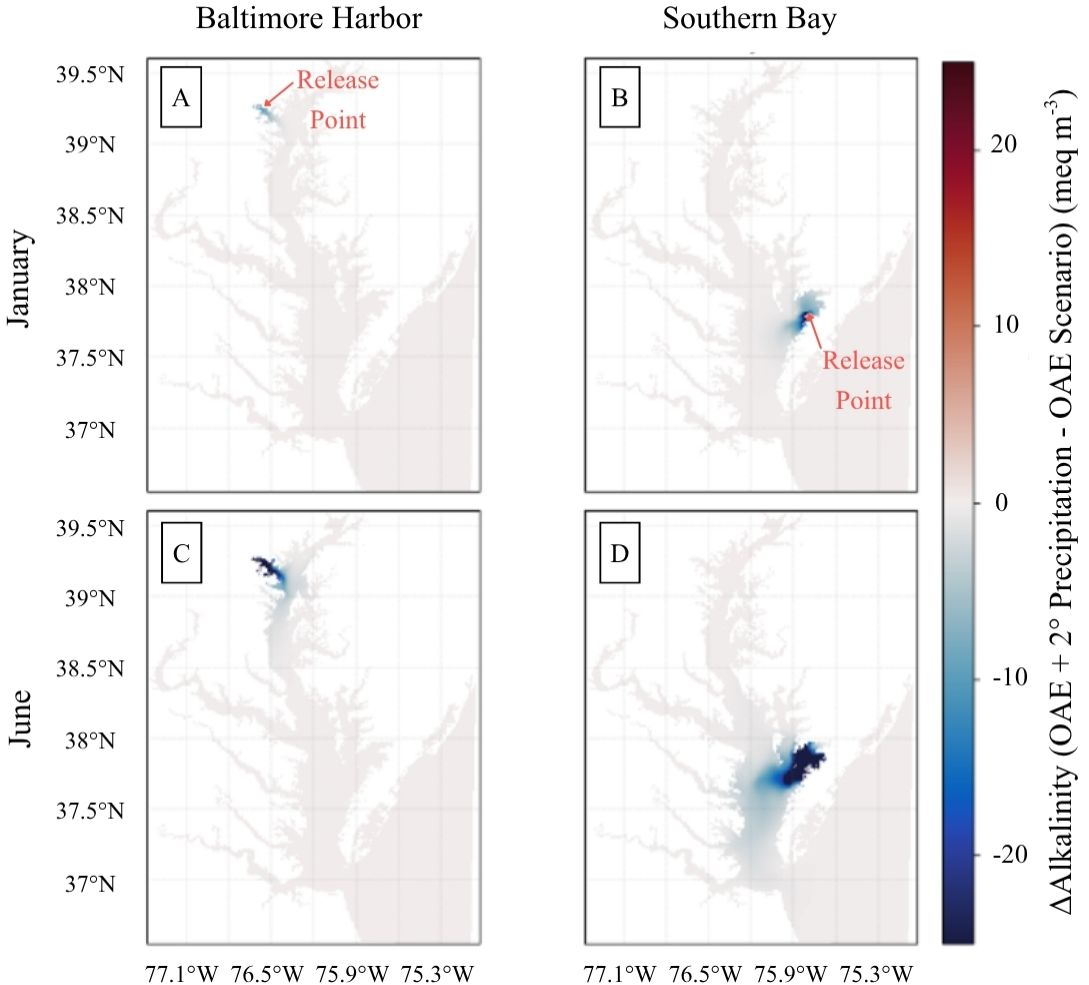




	Exp1 3h Filtered	Exp1 24h Filtered	Exp1 24h Unfiltered	Exp1 48h Filtered	Exp2 3h Filtered	Exp2 24h Filtered	Exp2 24h Unfiltered	Exp2 48h Filtered
Mg	11.98	1.83	1.41	1.02	100.00	72.02	55.66	7.12
Ca	88.02	98.17	98.59	98.98	0.00	27.98	44.34	92.88




A
January
B
June
ΔAlkalinity (meq m-3)
8
6
4
2
0
-2
-4
-6
Jan
05
09
13
17
21
25
29
Feb
10
0
-10
-20
-30
-40
-50
-60
29
Jun
05
09
13
17
21
25
29
Jul
Baltimore Harbor: OAE
Baltimore Harbor: OAE + 2° Precip
Southern Bay: OAE
Southern Bay: OAE + 2° Precip


Baltimore Harbor
Southern Bay
January
June
A
B
C
D
Release
Point
Release
Point
39.5°N
39°N
38.5°N
38°N
37.5°N
37°N
77.1°W
76.5°W
75.9°W
75.3°W
20
10
0
-10
-20
ΔAlkalinity (OAE + 2° Precipitation - OAE Scenario) (meq m-3)

Supplementary Files

This is a list of supplementary files associated with this preprint. Click to download.

- ARPAPEWATERCHEMDATAALLV4.xlsx
- SuppMaterialsSavoieNCEE.docx